2011

Resonant Antennas Based on Coupled Transmission-Line Metamaterials

Christopher S. Merola
University of Massachusetts Amherst

RESONANT ANTENNAS BASED ON COUPLED TRANSMISSION-LINE METAMATERIALS

A Thesis Presented

by

CHRISTOPHER S. MEROLA

Submitted to the Graduate School of the
University of Massachusetts Amherst in partial fulfillment
of the requirements for the degree of

MASTER OF SCIENCE IN ELECTRICAL AND COMPUTER ENGINEERING

May 2011

Electrical and Computer Engineering

RESONANT ANTENNAS BASED ON COUPLED TRANSMISSION-LINE METAMATERIALS

A Thesis Presented

by

CHRISTOPHER S. MEROLA

Approved as to style and content by:

Do-Hoon Kwon, Chair

Daniel H. Schaubert, Member

Marinos N. Vouvakis, Member

C. V. Hollot, Department Head
Electrical and Computer Engineering

ACKNOWLEDGMENTS

I could not have completed this work without the assistance of many people. I would first like to thank my advisor Prof. Kwon for giving me the opportunity to be his student in the lab. His ideas and support have guided me in learning how to perform research effectively, and his patient help with writing and revisions has been invaluable. I would also like to thank Prof. Schaubert for bringing me into his lab to work while I was an undergraduate, and introducing me to the world of antenna design. His office door has always been open and inviting of my questions. I thank Prof. Vouvakis for sparking my interest in electromagnetics while teaching Fields and Waves, and also for his daily words of wisdom over lunch at the Bluewall. Additionally, I thank the students of the Antennas and Propagation Lab for support, discussion of topics and ideas (engineering related or otherwise), and for keeping the lab fun. In particular, I would like to thank Steve Holland for playing the role of my "big brother" in the lab and taking the time to help me when I have been confused or stuck. And lastly, I could never have accomplished what I have without the love and support of my family along my meandering journey through life.

ABSTRACT

RESONANT ANTENNAS BASED ON COUPLED TRANSMISSION-LINE METAMATERIALS

MAY 2011

CHRISTOPHER S. MEROLA

B.S.E.E., UNIVERSITY OF MASSACHUSETTES AMHERST

M.S.E.C.E., UNIVERSITY OF MASSACHUSETTS AMHERST

Directed by: Professor Do-Hoon Kwon

A novel microstrip patch antenna topology is presented for achieving a dual-band response with arbitrarily closely spaced resonances. This topology is based on a coupled transmission line structure in order to take advantage of the separation in propagation constants for parallel (even-mode) and anti-parallel (odd-mode) current modes. Applying a metamaterials inspired design approach, periodic reactive loadings are used to design the underlying transmission line to have specific propagation constants necessary to realize a desired separation between two resonant frequencies. Using a single probe feed for a finite coupled line segment, both even- and odd-mode resonances can be excited to radiate efficiently at their respective design frequencies. The efficiency of the odd-mode radiation is enhanced by separating the two lines, while strong coupling is maintained by inserting a series of narrowly-separated thin loops between them. Several example resonant antenna designs, in the 2.45 GHz band, are presented.

The directivities of these microstrip patch antennas are enhanced by optimizing the physical length of the resonant structure. For a resonant antenna obtained by cascading several unit cells of reactively loaded microstrip segments, dispersion analysis is employed for the unit-cell design. Maximum directivity is achieved by choosing the overall physical length to be slightly less than a half wavelength in free space at the design frequency. This gain optimization is applied to three coupled-line antennas, as well as a single resonance patch. Excellent agreement is observed between simulated and measured responses across all designs.

The potential of loading the coupled line structure with active components is also explored. Varactor diodes are placed on coupled-line structures in two configurations. In one configuration, both resonant frequencies are affected. In the other configuration, only the odd-mode characteristics are reconfigured. In this way, the resonant frequency of either one or both modes can be adjusted by applying a DC bias voltage to the varactor diode loading elements. Two antennas, one employing each of these topologies, were designed and fabricated. Control of the resonant frequency over the predicted range through applying a bias voltage is observed with the fabricated prototypes.

TABLE OF CONTENTS

LIST OF FIGURES

Figure **Page**

CHAPTER 1

INTRODUCTION

1.1 Overview

Planar printed antennas have been studied extensively due to the availability of simple, low-cost fabrication and easy integration with other electronic components using printed circuit technologies. The most popular printed antennas are microstrip-patch, although they typically suffer from poor gain and narrow bandwidth. Many design methods have been investigated to tackle these short comings [1]. Stacking elements by increasing the number of dielectric and conductive layers has been demonstrated as an effective method to achieve an increased bandwidth [2] and a higher gain[3]. Although this method can significantly broaden the bandwidth and attain a gain as high as 10 dBi, it adds size, weight, and fabrication complexity. Building a patch on an air substrate can improve the gain and bandwidth, but the structure must be supported by posts or foam pads, making the antenna fragile and more difficult to feed[4, 5]. One method for improving gain while using a single-layer substrate involves surrounding the patch with a photonic band-gap substrate to suppress surface waves[6]. This has been shown to give a gain increase of 1.61 dB, but it effectively increases the antenna size to over $2\lambda_0/3$ in both length and width in terms of the free space wavelength λ_0. Another method uses a patch partially supported by dielectric and partially over air, which results in intermediate performance parameters between those using either substrate [7].

Pattern and frequency reconfigurable microstrip antennas have been reported for usable bandwidth or signal-to-noise performance increase. For example, the idea

of reactive loading in order to reconfigure pattern, frequency, and polarization of a patch design was introduced in [8]. This method makes use of tunable reactive loading for frequency reconfiguration and higher order modes for pattern diversity. Loading specific resonant modes through a careful choice of load locations has also been used to design a frequency reconfigurable slot antenna[9]. Although this design has wide frequency tuning ranges for both bands, it has a low gain of between -0.6 and 1.8 dBi depending on the resonance under consideration and the DC bias. Modifying line lengths electrically to switch the radiation direction of a printed Yadi-Uda antenna has been demonstrated in [10, 11]. Using MEMs switches to implement pattern, frequency, and/or polarization shows an excellent promise [12, 13, 14, 15]. MEMs exhibit low loss, low power consumption, and can operate at high frequencies and power levels. Unfortunately, they are complex to fabricate, expensive, and have a high reactive loading relative to comparable technologies [16]. The pattern and frequency reconfigurable designs realized by our topology employing varactor diode loads are more limited in capability, having narrow tuning range and only a few potential patterns. In addition, varactor diodes have higher loss and available circuit models are typically limited to frequencies at or below X-band [17]. However, our designs feature lower cost of fabrication, much simpler DC control networks, and continuous, rather than discrete, tuning capabilities.

In this study, resonant antennas are designed based on a transmission line (TL) metamaterial design approach [18]. The novel antenna design utilizes a coupled TL structure in order to obtain two un-coupled resonances whose frequencies can be adjusted independently of each other. Any currents flowing on the coupled structure are described as a properly weighted superposition of even (parallel) and odd (anti-parallel) current modes. A method is presented to independently control the phase velocities of these modes in order to obtain a structure with two resonances. Additionally, the phase velocity is modified such that the antenna is resonant at a length

which achieves optimal gain for a patch antenna. Several resonant printed antennas are designed based on the design approach, featuring either dual-band, wide-band, or frequency-reconfigurable characteristics. A single patch with optimal gain is also presented in order to demonstrate the gain optimization technique independent of the coupled line structure. Prototype antennas are fabricated and their measured characteristics are compared with numerically simulated predictions.

1.2 Periodic Loading

1.2.1 Controlling Resonant Frequency Separation

The difference between even- and odd-mode current directions causes each mode to have distinct TL parameters. This results in different propagation constants for the even-mode β_e and odd-mode β_o. Applying this phenomenon, a dual-band patch can be built with resonances associated with the two propagation constants. Smaller spacing between the coupled lines results in higher coupling and a larger separation between resonances. This design approach relies on strong coupling between the two TLs in order to have an appreciable propagation constant separation between the modes. Unfortunately, odd-mode currents for two very closely spaced elements do not radiate efficiently. For efficient radiation to occur in both modes, strong coupling must be maintained between the lines across a wide physical separation. To accomplish this, a coupling loop structure was placed between two wide TL segments, or patches, leaving a small gap along the symmetry plane. The separation between the even- and odd-mode phase velocities is controlled by the difference in the capacitances that this structure exhibits in each of these modes. In the even mode, the symmetry plane results in the end of the loop being closely spaced to a perfect magnetic conductor (PMC) boundary. The boundary condition along the symmetry plane in the odd-mode instead places an effective perfect electric conductor (PEC) boundary. The close spacing between the end of the loop and the ground plane creates a significant

increase in the capacitance of the structure. This increase in capacitance only affects propagation of the odd mode, separating even- and odd-mode electrical lengths for the same physical length l. A separation between resonances of 3.66% at 2.405 and 2.489 GHz has been achieved on a single layer 62 mil-thick Duroid 5880 substrate. Using a narrow separation between resonances, a wide impedance bandwidth design has also been designed and measured having an $S_{11} < 10$ dB bandwidth BW = 1.4%.

1.2.2 Maximizing Directivity

In addition to engineering a coupled-line structure to obtain resonances at two desired frequencies, this work describes usage of a unit-cell design in order to optimize the directivity of a patch antenna. This is accomplished by choosing a physical patch length which achieves the maximum directivity at the desired frequency, then modifying the propagation constant of the microstrip such that the patch is resonant at this frequency. Optimum gain is achieved when the patch has a length equal to one-half wavelength in free space. A method is described to match the propagation constant of the microstrip TL to that of free-space at the resonant frequency, maximizing directivity of the patch antenna.

Simulation and measurement results for a single resonance patch utilizing this technique and operating at 2.45 GHz are presented. A gain improvement close to 1.5 dB is achieved over traditional patches on the same substrate. Applying this method to the coupled designs, realized gains for the even-mode up to $G_R = 9.3$ dBi and for the odd-mode up to $G_R = 7$ dBi were measured.

1.2.3 Loading with Active Components

Also explored in this study is the potential to reconfigure one or both modes of a coupled-line patch by use of varactor diodes. These diodes act as variable capacitors. The diode capacitance is controlled by the reverse voltage applied across its terminals. Varactor diode loading allows the patch resonance to be tuned with a DC bias voltage.

Two possibilities utilizing varactor loading are explored. In the first configuration, diodes are placed such that they load both modes. By properly tuning the frequency separation between these resonances it is possible to design an antenna where either even- or odd-mode resonance can be selected at the design frequency. These two modes have different radiation patterns, as will be described in Subsection 2.1.1. A particular design which allows either pattern to be selected at 2.45 GHz is presented. In the second diode configuration, only the odd mode is affected by the varactor loading. In this way, it is possible to keep one resonant frequency constant while tuning the second resonance through a DC offset. Using this layout, an antenna is designed with a fixed even-mode resonance at 2.45 GHz, and an odd-mode resonance that can be swept between 2.8 to 2.9 GHz.

CHAPTER 2

ANTENNA TOPOLOGY

2.1 Coupled Lines as Antennas

2.1.1 Even- and Odd-Mode Decomposition

Computationally, the even- and odd-mode coupling can be efficiently modeled and analyzed using either a perfect magnetic conductor (PMC) or perfect electric conductor (PEC) boundary down the symmetry plane between the lines [19], as illustrated in Fig. 2.1(a). As the spacing between the lines is narrowed, the distance from either transmission line to this symmetry plane decreases and coupling is increased. The electric (odd mode) or magnetic (even mode) coupling can be represented as periodic, shunt reactive elements. Differences in these element values can cause the even- and odd-mode phase velocities to be different.

Fig. 2.1(a) shows the top view of typical coupled transmission lines of finite length. The even- and odd-mode currents exhibit the distinctly different radiation patterns shown in Fig. 2.1(b). In the even-mode, the symmetric current distribution has the radiation pattern characteristic of a two-element broadside array. Since the odd mode requires currents on the two patches to be 180° out of phase, the resulting pattern has a broadside null with two lobes steered to an angle determined by separation between elements. This quality can be of use for certain applications. Changing radiation pattern to avoid interference or eavesdroppers is possible by switching between modes. Combining the patterns can be used to steer location of the main beam or a null.

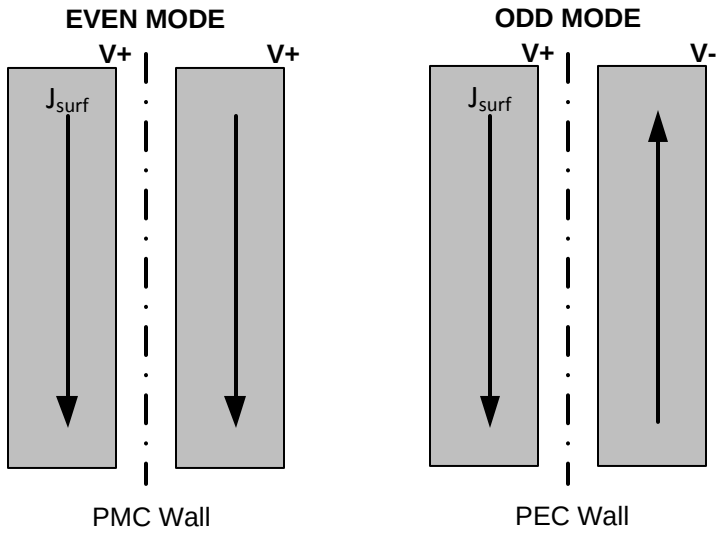

(a)

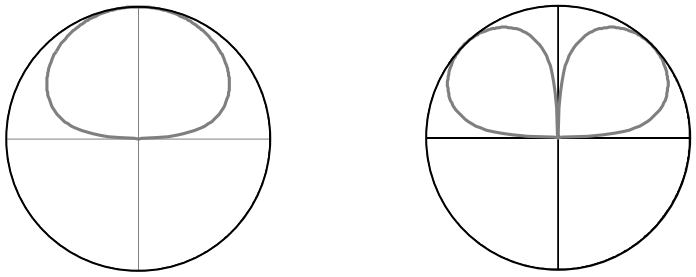

(b)

Figure 2.1: Current flow and radiation characteristics of the even- and odd-modes of a coupled structure. (a) Top view of the even- and odd-mode currents, and the effective boundary conditions from symmetry. (b) Typical H-plane radiation patterns associated with these current modes.

2.1.2 Coupling Loops

In order to achieve the desired difference in propagation velocity between even- and odd-modes of microstrip coupled lines, the lines must be placed in close proximity. The odd-mode, however, does not radiate efficiently when the radiating elements are placed so close to the symmetry plane. To solve this problem, a coupling structure was placed between two wide transmission line segments, or patches. This structure takes the form of narrow loops extending off the inner edge of each patch toward its neighbor, separated by a small gap g, along the symmetry plane. The coupling loops can be seen between the lines in the unit-cell diagram shown in Fig. 2.2. The narrow line width reduces unwanted radiation from this portion of the antenna, while increasing coupling by forcing the currents to flow close to the coupled edge. From a circuit perspective, the loop loads the patch similarly to a open-circuited shunt stub. The stub used is less than $\lambda/4$ long, giving it a capacitive input reactance. The separation in the even- and odd-mode phase velocities is created by the difference in capacitance that this structure exhibits in each of these modes. In the even-mode, the symmetry plane results in the end of the stub being closely spaced to a PMC boundary. This effective open forces the fringing field to zero, slightly shortening the electrical length of the stub. This has little effect on its capacitance versus the stub with no PMC boundary. In the odd mode, however, the PEC boundary places an effective ground plane very close to the end of the stub. The close spacing between the end of the stub and the ground plane creates a significant increase in the capacitance of the stub. This increase in capacitance only affects propagation of the odd mode, separating even- and odd-mode electrical lengths for the same physical length l_c.

The difference in electrical lengths can be controlled by adjusting the ratio of the even-to-odd mode capacitances. This is primarily controlled by two parameters: the gap g between the coupling loops and the length l_c of the coupling edge. Figs. 2.3(a) and 2.3(b) plot the dispersion curves for different values of l_c (for a fixed g) and for

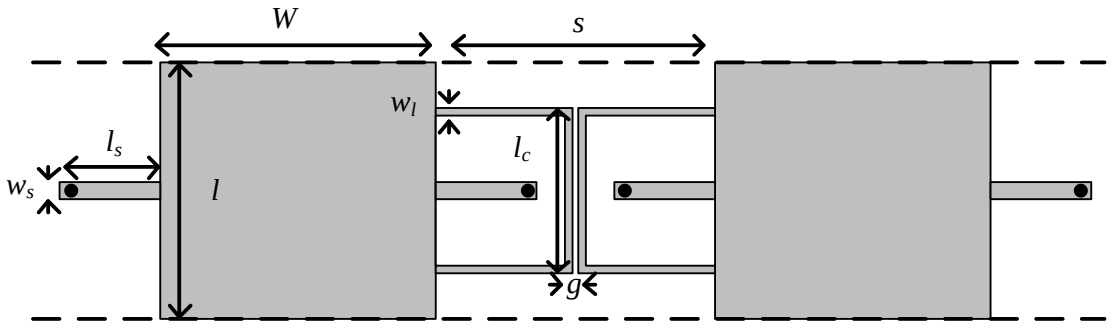

Figure 2.2: Unit cell diagram for the coupled-line patches. Dashed lines indicate periodic cell boundaries.

different values of g (for a fixed l_c), respectively. Decreasing g or increasing l_c will increase the phase constant separation. Changes in g have a negligible effect on the even-mode capacitance. A larger l_c lowers the impedance of the equivalent open-circuit stub. This has some effect on the even-mode capacitance, but much less than that of the odd-mode. By adjusting these two parameters, it is possible to tune the difference in even- and odd-mode phase velocities.

2.2 Gain Enhancement Using Shunt Inductive Stubs

The ends of a patch antenna perpendicular to current flow are primary radiating components of the structure. These form slots between the edge of the conducting trace and the ground plane. Due to this fact, the patch can be modeled as a magnetic dipole at the location of each radiating edge. This determines the pattern in the H-plane, allowing directivity to be increased with patch width (slot length). However, in the E-plane this forms a 2-element array with separation determined by patch length. The directivity of this 2-element array is maximized when the element spacing is $\lambda_0/2$. This means that a patch will have optimum directivity if it is resonant at this length. Additionally, at this length the pattern will have narrower E-plane beamwidth, with deep nulls on the horizon. Unfortunately, this length matching condition is normally only met when air is used as the substrate. Since the propagation constant β is

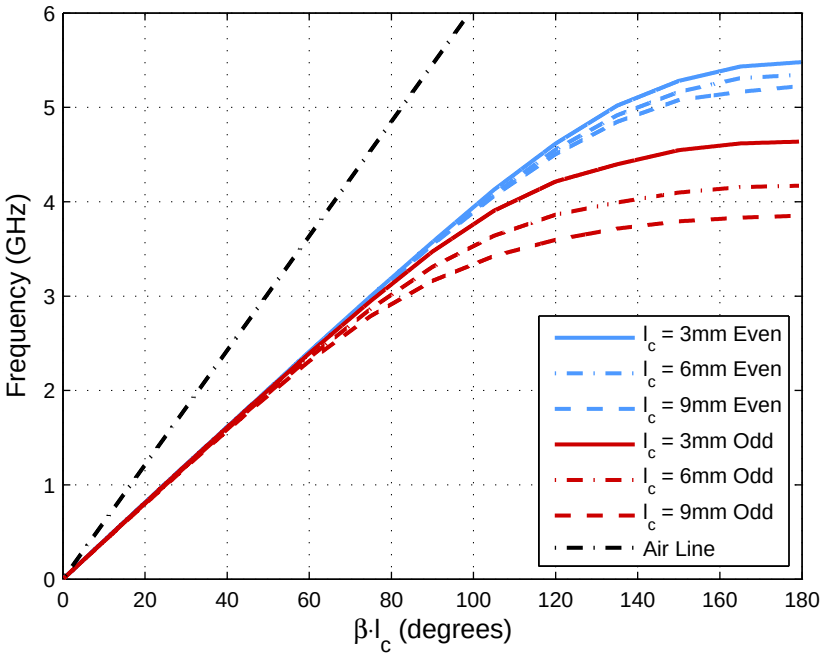

(a)

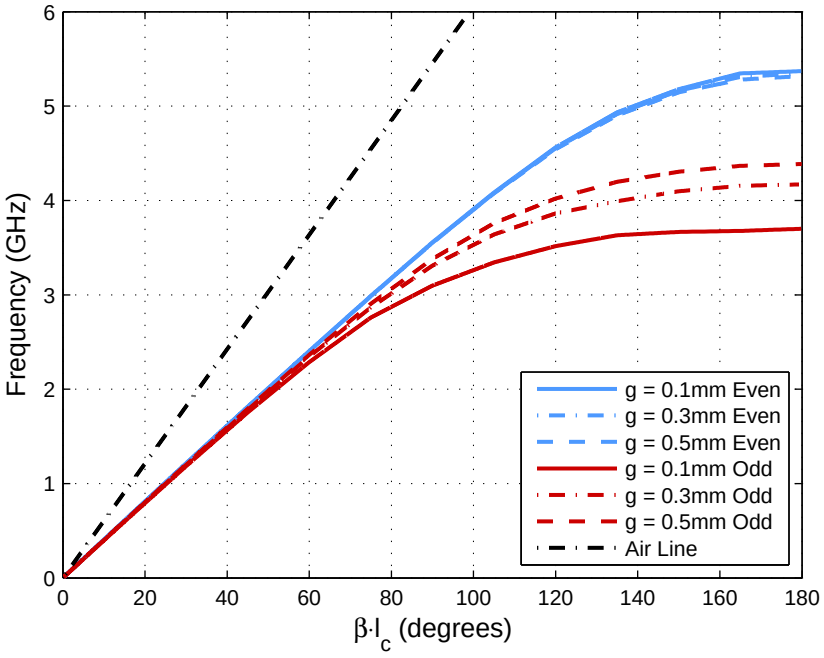

(b)

Figure 2.3: Coupling loop parameters and their effect. (a)Effect of the coupled edge l_c on the dispersion relation. The gap g is fixed at 0.3 mm. (b) Effect of the coupled loop separation g on the dispersion relation. The coupled edge l_c is fixed at 9 mm.

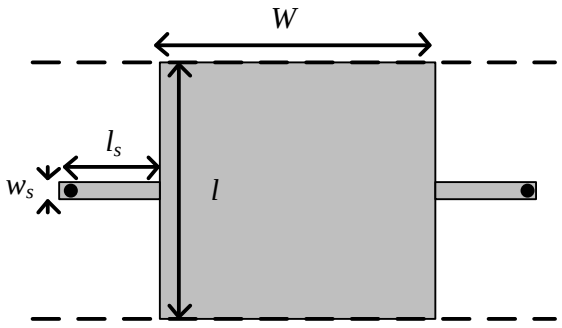

Figure 2.4: Unit cell diagram for the maximized-gain patch. Dashed lines indicate periodic cell boundaries.

increased as substrate permittivity is increased, a microstrip patch will be resonant at a shorter-than-optimal length. This section describes a method of decreasing β on the patch such that it matches that of free space. The propagation constant on the underlying TL of the patch is engineered in order to realize the maximum directivity.

In order to design a patch that has maximum directivity at resonance, β of the structure must be controlled. This is accomplished by designing the unit cell for an infinite periodic structure with the desired β. Fig. 2.4 shows the unit cell used for the single resonance patch with maximized gain. The dashed lines represent the periodic boundary conditions. The via-terminated stubs on either side provide shunt inductance L_s, which decreases β. In order to realize small values of L_s, stubs are placed on both sides of the patch in parallel.

Placing a series capacitance on the patch would affect β similarly; however, that method has several draw-backs. Interdigital capacitors require narrow gaps cut into the trace layer, creating a geometry that takes longer to solve due to computational intensity. Also, in order to realize a large capacitance, the gaps become such a small fraction of a wavelength that they begin to push both the limits of the FEM solver and that of fabrication tolerances. Even if these difficulties are overcome, placement options for a probe feed become limited, creating difficulty in matching the antenna to the line. Due to these issues, shunt inductors were chosen instead.

Shunt inductors have limitations as well. As the patch width is increased, shunt capacitance of the TL will become large resulting in an L_s value too small to be realized. L_s is decreased as the stub is made shorter. At a point, the necessary stub will be so short that the length is comparable to the width. Here, the shorted stub model breaks down, and very small variations in stub length have a large effect on impedance. Having two stubs in parallel (one on each side) helps with this, but still results in a trade off between beamwidths in the E- and H-planes. Another solution is to narrow the width W of the patch, decreasing the inherent shunt capacitance of the microstrip structure. Adjusting W results in a trade-off with gain and bandwidth, both of which increase with larger W.

CHAPTER 3

PATTERN- AND FREQUENCY-RECONFIGURABLE DESIGNS

3.1 Varactor Loaded Lines

For the resonant coupled-patch antennas under consideration, modifying shunt loading of the lines will change the resonance frequencies. Reverse-biased varactor diodes can be used as variable capacitors [19] allowing tunable resonances. The resonances will shift down in frequency as shunt capacitance is increased. The shunt capacitance can be reconfigured using variable capacitors in either a shunt path from a patch to the ground [Fig. 3.1(a)], or placed between the two lines [Fig. 3.1(b)]. In the first configuration, the diodes will affect both modes, whereas placing the diodes across the symmetry plane, as in the second configuration, affects the old-mode only. The value of the capacitance can be adjusted easily by varying a DC bias voltage.

In order to predict the effect of the varactor diode in numerical simulations, a simplified model was used. The Skyworks Sollutions, Inc SMV1234-07LF diode was

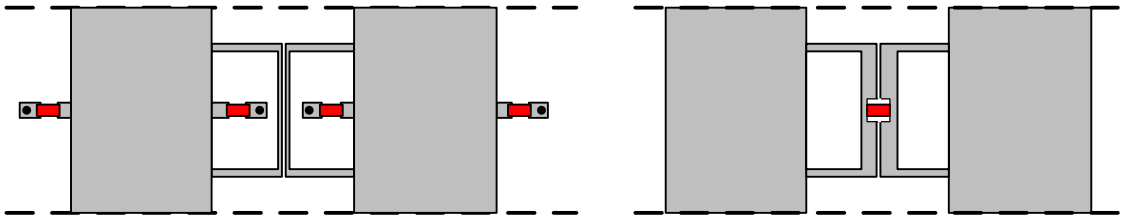

(a) (b)

Figure 3.1: Unit-cell layouts of reconfigurable designs. Diode placement marked in red. (a) Pattern reconfigurable unit-cell. (b) Odd-mode frequency reconfigurable unit-cell.

considered as a series RLC circuit. The variable capacitance of this model has a capacitive range of $C_d = 1.32$ pF at 15V to 9.63 pF at 0V. The package inductance $L_d = 0.7$ nH and diode loss $R_d = 0.8\ \Omega$ are also taken into account in this model. The small L_d placed in a shunt configuration increases resonant frequency. The loss due to R_d can have a significant impact on both impedance matching and gain. Resonance tuning using this method is limited due to a diminishing effect as the capacitance becomes larger. In this way, a diode with a very large range will not necessarily allow wide tunability. Such a diode will, however, be more sensitive to small voltage changes. The SMV1234-07LF was chosen for its range of C_d and its rating for operation up through 2.5 GHz.

Bias voltage for pattern and impedance measurement was applied through the coax feed probe. This was accomplished using the Agilent E8363B network analyzer, which allows for DC input to be applied from an external voltage source. EPCOS, Inc B82496C3470J 47 nH inductors were used as RF chokes on other necessary DC interconnects.

3.2 Pattern Reconfigurable Antenna

In order to realize a pattern reconfigurable design, varactor diodes were placed on the shunt stubs to ground, as shown in Fig 3.1(a). This arrangement of varactor diodes affects the even- and odd-modes almost equally. Therefore, the entire resonance curve that includes both resonances will shift up or down in the frequency axis as a function of the DC bias voltage. The resonances are separated such that, at one capacitance value, the odd-mode is resonant at the design frequency. By decreasing voltage (increasing capacitance), the even mode can be configured to resonance at the same frequency. In order to obtain clear even- and odd-mode patterns the resonances should be spaced apart as far as possible. Closer spacing of the resonances will cause the pattern to fade between that of the even and odd-mode as bias is adjusted. In

this case the even-mode radiation is dominant and the effect is voltage adjustable beam squint.

The bias setup for this configuration was accomplished by applying a positive DC voltage to all of the diode cathodes. The anodes were attached to stubs terminated in a via to the ground plane. The bias voltage was applied to the driven patch through the feed probe and transfered to the parasitic patch through an RF choke. This was accomplished by placing a small rectangular trace near the coupling loops at one end of the patch. An inductor was placed between each loop and this trace in order to maintain the same DC potential at all diode cathodes.

3.3 Odd-mode Frequency Reconfigurable Antenna

When the varactor diodes are placed across the symmetry plane of the coupled structure as shown in Fig. 3.1(b), their loading only affects the odd-mode. In the even-mode, the presence of varactor diodes has minimal effect due to the effective open-circuit bisecting them. In the odd-mode, the effective ground plane bisecting the diodes causes the per-unit-cell line loading to be equal to $2C_d$, $L_d/2$, and $R_d/2$. Using this diode placement allows the frequency of the odd-mode resonance to be tuned without affecting the even-mode resonance.

The parasitic inductance of the varactor diodes has a significant effect on the separation between resonances. The small shunt inductance $L_d/2$ seen by the odd-mode has a larger effect on frequency separation than the coupling loop structure, limiting possible separations. To overcome this, diodes can be chosen for their package inductance to set the initial difference between β_e and β_o and the coupling loop could be used to fine tune the spread. The prototype of this design uses a diode we had already tested at this frequency, and accepted that the odd-mode resonance occurs in a range 300 MHz above that of the even mode.

CHAPTER 4

UNIT CELL DESIGN USING DISPERSION DIAGRAM

In this study, the overall antenna structure is obtained by cascading several identical building blocks, or unit cells. By cascading unit cells to attain 180° of total phase progression, a resonant antenna is constructed. The phase velocity along the transmission line is analyzed using a single unit cell under periodic boundary conditions. Fig. 2.2 shows the top view of the unit cell employed in this study. The symmetrical structure consists of two lines of the width W, separated by the distance s. Between these lines are coupling loops with the line width w_l, separated by a narrow gap g, along the symmetry plane. The length of the closely coupled edge between these loops is defined as l_c. Short-circuited shunt stubs of the width w_s and the length l_s extend from each side of the lines along at center of the unit cell length.

This section describes the methods used in unit cell design. Dispersion diagrams for the unit-cells of all designs are plotted and discussed. An approximate analytical model is presented in order to develop insight into how various parameters affect propagation in each mode. The process of cascading unit-cells to form a resonant antenna is discussed along with the ability to accurately predict resonant frequencies from unit-cell dispersion. Lastly, ability to excite both modes through a single feed is described along with a definition for the resulting input impedance.

4.1 Analytical Dispersion Model

Equation (4.1) shows how shunt periodic loading affects the electrical length βl of a unit cell. Although this is the correct formula for a periodically loaded line, consid-

ering the loops and stubs as a point load b at the center of the unit cell is an approximation. Let k_m and Z_m denote the wave number and characteristic impedance of the unloaded microstrip line used for the patch, respectively. Characteristic impedance and propagation constant for the TL of the shorted stub are denoted by Z_{s0} and β_s. These values for a TL of width l_c used for our simplified loop model are denoted by Z_{l0} and β_l. If we treat the structure as a one dimensional TL and consider the loops and stubs as point loads, the dispersion relation for the unit cell is given by [19]

$$\beta l = \cos^{-1}(\cos k_m l - \frac{b}{2}\sin k_m l), \tag{4.1}$$

where b is the total shunt reactance of the loop in the even- or odd-mode (Z_{le} or Z_{lo}) and the shunt stubs Z_s connected in parallel, normalized to Z_m. The impedances used for the analytical models in Fig. 4.1, 4.2, and 4.3 are defined by

$$Z_s = jZ_{s0}\tan\beta_s l_s, \tag{4.2}$$

$$Z_{le} = -jZ_{l0}\tan\frac{\beta_l(s-g)}{2}, \tag{4.3}$$

$$Z_{lo} = Z_{l0}\frac{(1/j\omega C_o) + jZ_{l0}\tan\beta_l l_c}{Z_{l0} + j(1/j\omega C_o)\tan\beta_l l_c}. \tag{4.4}$$

The value C_o used in Fig. 4.1 was determined using a quasi-static model of coupled MS lines [20]. These equations are used to solve for the additional odd-mode capacitance between the loops. This model utilizes conformal mapping in order to transform the structure into a parallel plate capacitor. The fields in the dielectric and in the air are considered separately, neglecting any fields which cross this boundary. Approximate per-unit-length capacitance is determined and then multiplied by l_c for the odd-mode loading of a single loop.

The model for the stub impedance Z_s gives good accuracy as can be seen in Fig. 4.3. The model used for the coupling loop is not as accurate due to its more complicated geometry. The analytical model of the coupling loop considers a simplified

structure of a wide TL stub terminated in an open-circuit for the even mode and C_o in the odd-mode. This model was found to give reasonable accuracy at low frequencies when the approximation of a point loading is good. As the frequency increases, the loop goes from being on the order of $\lambda/10$ to $\lambda/4$ and this approximation becomes invalid. This analytical model is not accurate enough to be used as a design equation, but gives good insight into the effect of the coupling loops. Fig. 4.1 and 4.2 include both numerically simulated and analytical solutions for the unit-cell dispersion of the dual-band and wide impedance bandwidth designs. Dispersion at lower frequencies is highlighted in Fig. 4.1(b) showing the fair accuracy of the analytical model in this range.

4.2 Accurate Prediction of the Resonant Length

In order to accurately predict patch resonance from unit cell prediction, fringing fields must also be taken into account [21]. These are the fields which extend beyond the ends of the patch, making the electrical length longer than that of the trace. For unit cell phase design, the electrical extension due to these fringing fields is more important than their physical extension. The fringing field depends on the width of the patch and the substrate chosen. The actual phase velocity of the line has a negligible effect. This means that the fringing length of a standard microstrip line can be used as a correction factor for metamaterial transmission-lines. Formulas for fringe length [21] give a physical length to be added which can be modified into an electrical length by multiplying by the wavenumber of the microstrip line. Alternately, a standard MS patch operating at the target frequency can be simulated. The electrical length of this patch as a transmission line gives the target phase length. Physical separation of radiating slots is also affected by fringing fields. The slot has been empirically determined to be located where the E-field along the ground plane has dropped to half-power (relative to the maximum at the end of the patch).

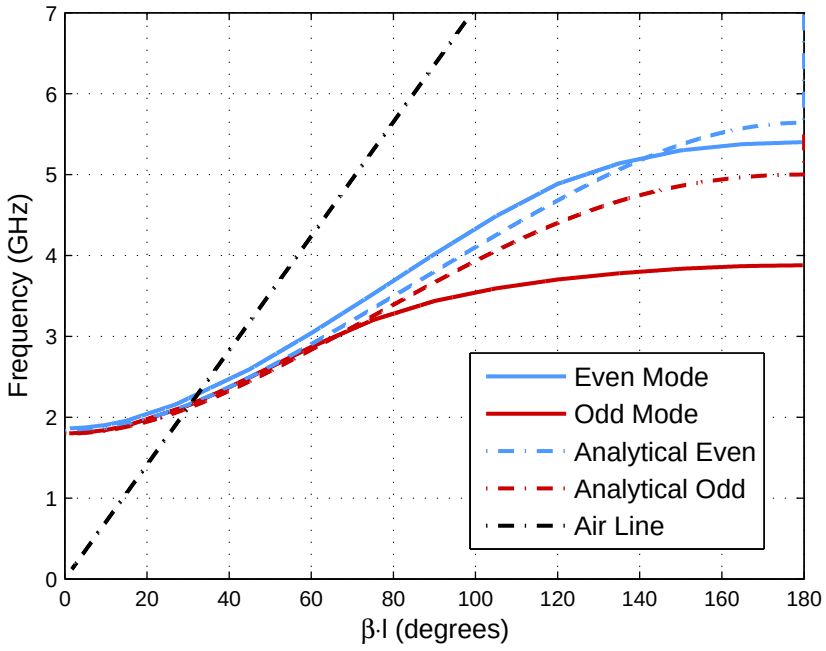

(a)

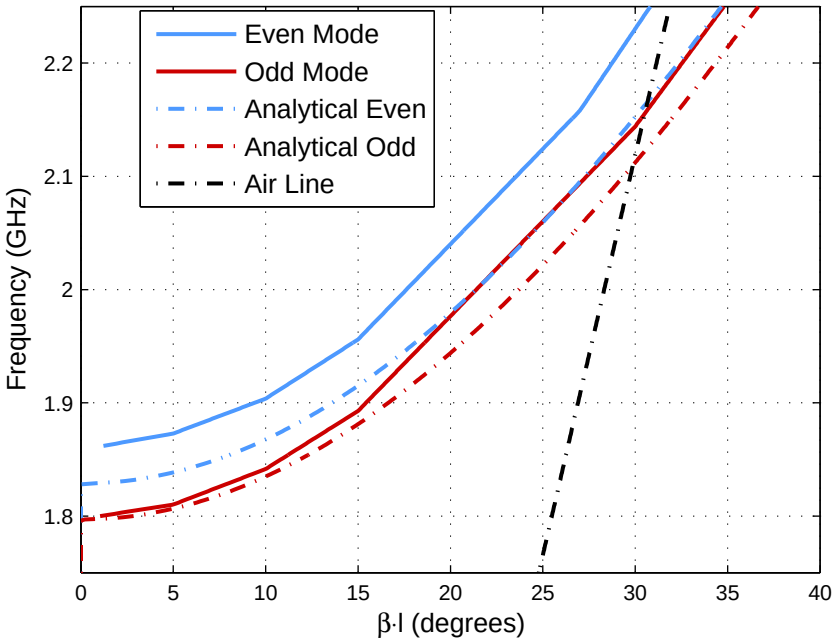

(b)

Figure 4.1: k-β diagram for a unit cell of the dual-band design. Numerical solutions, approximate analytical solutions, and the air line are plotted. (a) Full plot. (b) A magnified view over low frequencies for a better comparison of analytical and numerical results.

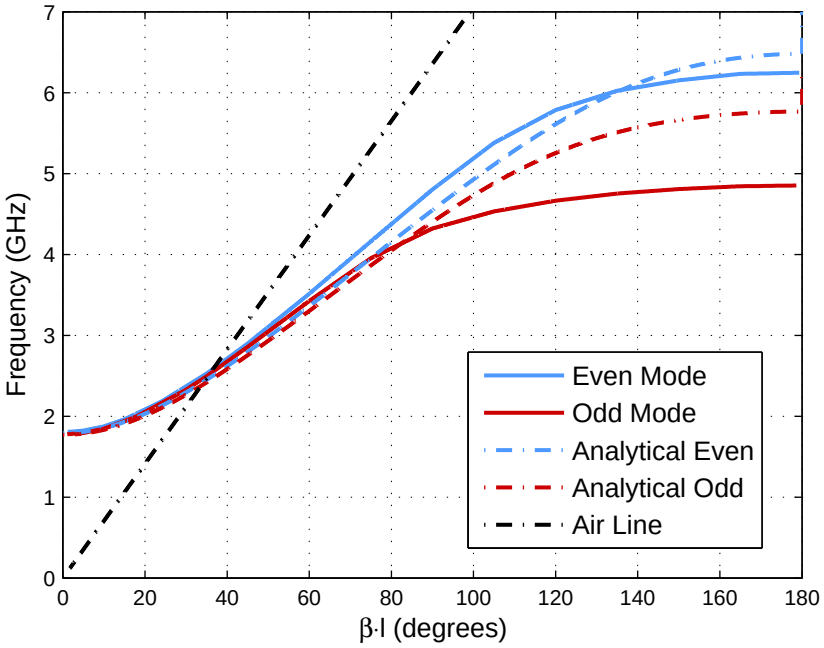

Figure 4.2: k-β diagram for a unit cell of the merged resonance design. Numerical solutions, approximate analytical solutions, and the air line are plotted.

The antenna designs presented in chapter 5 use a line width of 30 mm on a 62 mil thickness substrate of Duroid 5880 ($\epsilon_r = 2.2$). The fringing phase for this substrate was determined numerically by simulating a portion of an infinite line to be 11° total, 5.5° at each end. Dividing by the wavenumber gives a fringing length of 2.6 mm. From these numbers it is seen that the target unit cell phase is $169°/5 = 33.8°$. Subtracting the physical fringe length from λ_0=2 gives a target length 58.6 mm for maximum gain at 2.45 GHz. The fringe length determined using a numerical solver was found to be more accurate than the 7° predicted by the formula in [21]. The discrepancy is attributed to inaccuracy in the formula for microstrip lines with large width-to-height ratios.

The $k - \beta$ diagram for the single patch maximum-gain structure is plotted by the red line in Fig. 4.3. Also plotted are the $k - \beta$ diagrams for the same length, width, and substrate MS line, and free space k. It is shown that the MS line has a lesser slope and is below the air line at all frequencies, corresponding to a shorter physical

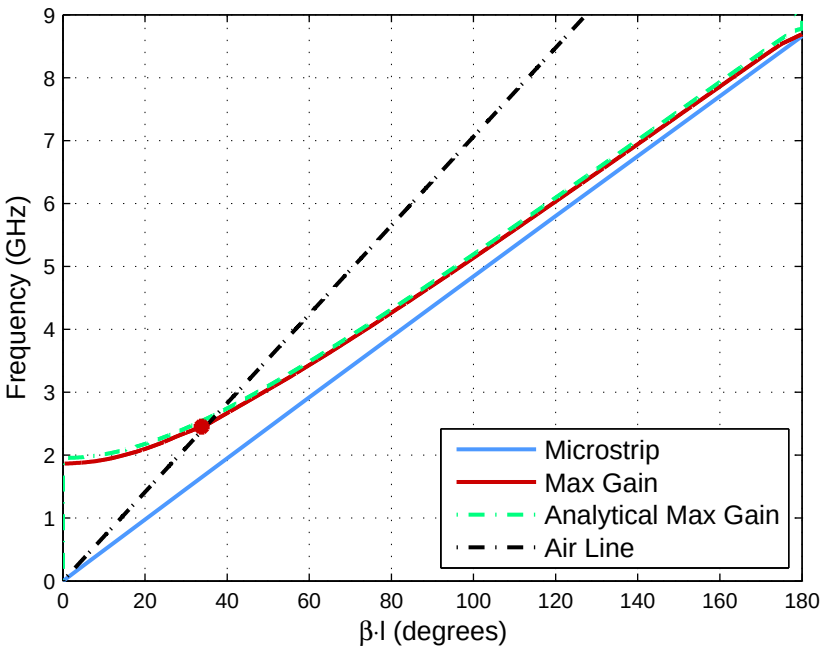

Figure 4.3: k-β diagram corresponding to the maximized-gain design (geometry given in Section 5.1), a standard microstrip patch of the same width, and free-space propagation. The green line represents an analytical solution for the stub loaded transmission line. The red dot marks predicted resonance for a 5-cell patch.

resonant length. The maximum directivity line is essentially a high-pass filter and is in a stop band at low frequencies. When the pass-band begins, β is above that of free-space with a gradual slope that will eventually converge to that of the MS line. The max-directivity and air lines intersect at 180° because of the design methods outlined in the previous section. Note that the reason this intersection occurs above the 2.45 GHz target frequency is due to the fringing field length.

Although bandwidth of a patch on an air substrate is greater than a similar patch on a dielectric, bandwidth is not improved by utilizing the proposed technique. The reason for this can be seen by observing the slopes of the lines in Fig. 4.3. The steeper the slope of a structures $k - \beta$ line a greater range of frequencies will have a similar phase length. When applied to a resonant structure, this means a larger frequency band is close to resonance, resulting in wider bandwidth. The air line

has a steeper slope then the MS line, implying greater bandwidth. Near resonant length, the optimized design has a lesser slope than the MS line, implying a narrower bandwidth.

Dispersion characteristics of the reconfigurable designs are plotted over a narrower range of frequencies in order to highlight varactor tuning predictions. Results for the unit-cell of the pattern reconfigurable design are plotted in Fig. 4.4, with solid lines representing results with $C_d = 4.2$ pF and dashed lines representing $C_d = 5$ pF. These C_d values correspond to odd- and even-mode resonances occurring at 2.45 GHz as predicted by numerical simulation of the full patch. The unit-cell design instead predicts odd-mode resonance to occur at 2.46 GHz and even-mode resonance at 2.477 GHz. It does, however, predict that either resonance can be tuned to the same frequency when slightly larger values of C_d are used. The dispersion diagram of Fig. 4.5 displays the predicted response of the odd-mode reconfigurable unit-cell. It can be seen the even-mode dispersion is virtually unaffected by the change of C_d from 1 to 8 pF. Predicted resonant frequency is 2.443 GHz for this mode, 1.25% higher than the 2.415 GHz predicted by simulation of the patch. The predicted odd-mode tuning range is between $2.799 - 2.870$ GHz versus $2.784 - 2.876$ GHz for the patch simulation. These results show that the unit-cell predictions for the varactor loaded patches give a good approximation of antenna performance.

4.3 Antenna Construction Using Cascaded Unit Cells

This antenna design technique involves designing a unit cell to have the desired propagation characteristic, then cascading a number of these unit-cells to create a resonant patch, as shown in Fig. 4.6. The first consideration is to determine how many unit cells to use, and then design the unit cell phase progressions to achieve the desired even- and odd-mode phase difference. First, choose the two desired resonant frequencies. Next, choose the length of the antenna L to be close to half of the free

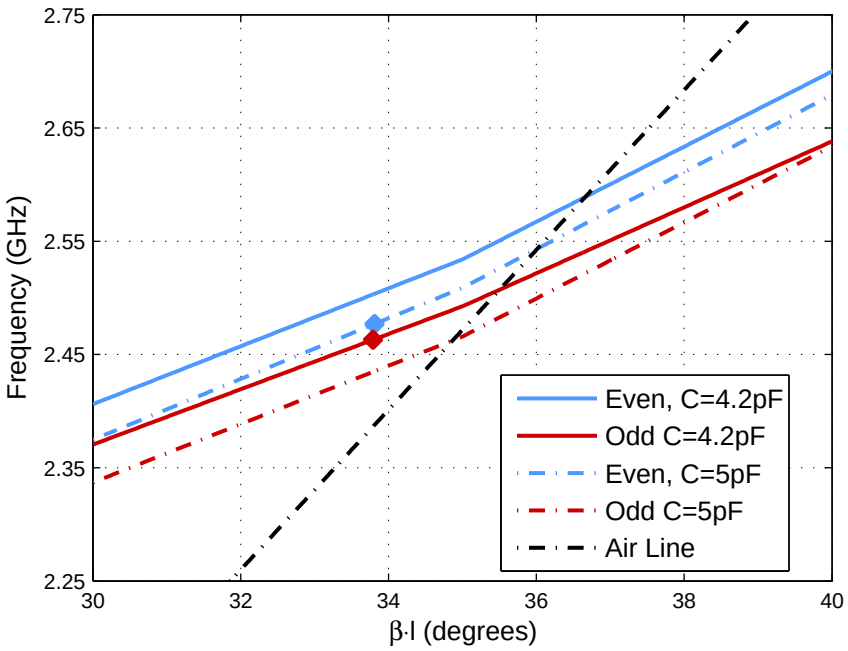

Figure 4.4: k-β diagram for a unit cell of the pattern reconfigurable design. Magnified region plotted to highlight tuning of both modes. The two dots indicate predicted resonance frequencies for a five cell antenna at $\beta l = 33.8°$.

space wavelength in the operating band. Dividing this length by the number of unit cells gives the unit cell length l. The designs presented in this paper use either 4 or 5 unit cells. The number of unit cells will be decided by the desired separation between resonances. For a greater separation between resonances, l_c must be made longer. It is desirable to make the unit cells as short as possible, while fitting in the necessary length of l_c.

The spacing s between the two patch elements will control the gain of both modes. If the elements are very close together, the odd mode will not radiate efficiently. As the elements are spaced further apart, the gain for both modes will increase, although the even-mode gain will increase more than the odd-mode gain. The designs presented were optimized to keep the gains of the two modes as close as possible. For this purpose, elements are spaced just far enough for the odd mode to radiate efficiently.

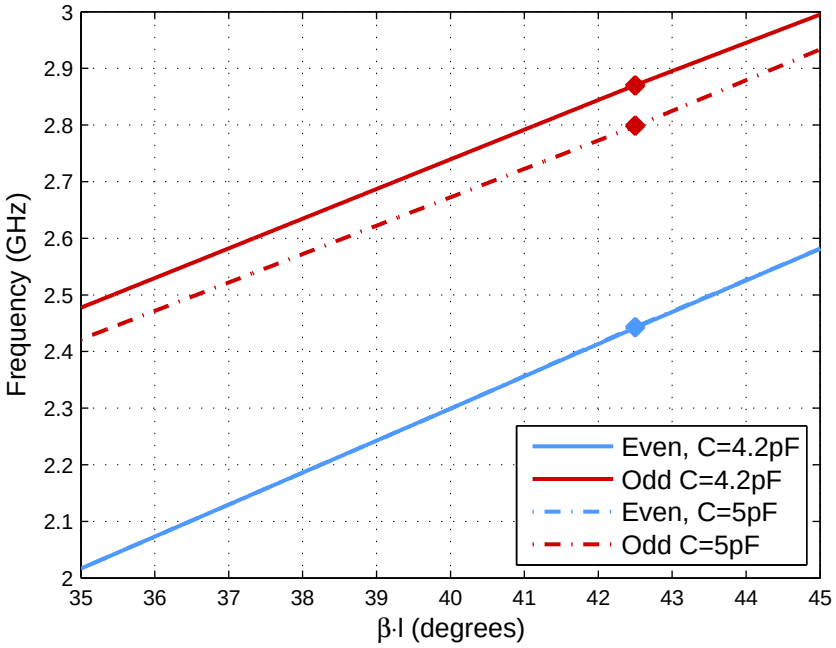

Figure 4.5: k-β diagram for a unit cell of the odd-mode reconfigurable design. Region plotted to show tuning of odd-mode without affecting even mode. The dots indicate predicted resonance frequencies for a four cell antenna at $\beta l = 42.25°$.

As the value of s is increased beyond this point, the gain imbalance between the two modes is also increased.

Once the general dimensions of the unit cell have been decided, the HFSS eigenmode solver is used to determine the even- and odd-mode electrical lengths of the unit cell. This is accomplished by placing a master/slave boundary condition along the dashed lines in Fig. 2.2. The phase is set to the resonant length divided by the number of unit cells. Due to the H-plane symmetry of the design, the even mode is computationally equivalent to simulating one half of the unit cell with a PMC boundary placed along the symmetry plane. Replacing this with a PEC boundary is computationally equivalent to the odd mode excitation. This simulation will predict the even- and odd-mode resonant frequencies of the antenna.

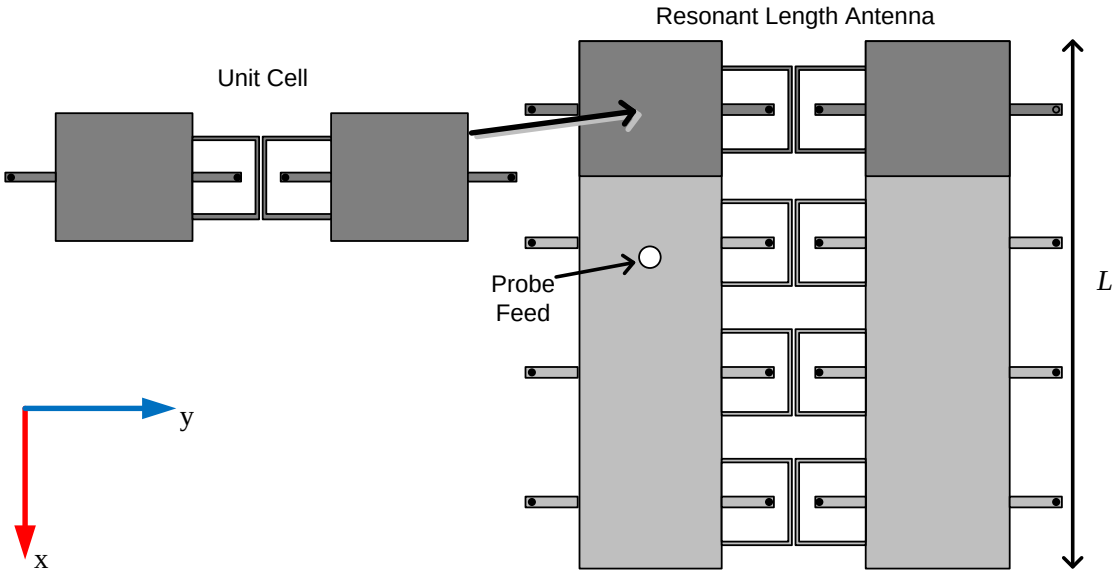

Figure 4.6: Cascading unit cells to form a resonant antenna.

4.4 Input Impedance of a Single Probe Excitation

In order to use this patch as a dual-resonance antenna, both modes must be simultaneously excited. Use of a probe feed on each patch allows an arbitrary excitation of the two modes. It is shown in (4.5)-(4.8) that exciting the antenna only at one port with the second port open-circuited makes the antenna input impedance Z_{in} to be simply a sum of the individual mode impedances Z_{ee} and Z_{oo} for the even- and odd-modes, respectively. Due to the uncoupled nature of the two modes, it follows that $Z_{eo} = Z_{oe} = 0$. Using this arrangement, the antenna can be fed with a single feed probe to either patch.

$$\begin{bmatrix} V_1 \\ V_2 \end{bmatrix} = \begin{bmatrix} Z_{11} & Z_{12} \\ Z_{21} & Z_{22} \end{bmatrix} \begin{bmatrix} I_1 \\ I_2 \end{bmatrix} \tag{4.5}$$

$$Z_{ee} = \frac{1}{2}(Z_{11} + Z_{12} + Z_{21} + Z_{22}) \tag{4.6}$$

$$Z_{oo} = \frac{1}{2}(Z_{11} - Z_{12} - Z_{21} + Z_{22}) \tag{4.7}$$

$$Z_{in}|_{I_2=0} = \frac{1}{2}(Z_{ee} + Z_{oo}) \tag{4.8}$$

CHAPTER 5

ANTENNA DESIGNS

Six antenna designs based upon the described technique are presented. They were chosen to operate in the 2.45 GHz band. All of the designs were built on a Rogers RT/Duroid 5880 ($\epsilon_r = 2.2$, $\tan\delta = 0.0009$) substrate of thickness 62 mil (1.57 mm) and a 0.5 oz (thickness of 0.017 mm) of copper cladding. A patch width of $W = 30$ mm and spacing of $s = 15$ mm were kept the same for all five of the coupled designs. The single patch used the same substrate, and W. The trace widths for the coupling loop structure and stubs in the unit-cell defined in Fig. 2 were set to $w_l = 0.5$ mm and $w_s = 1$ mm. The size of the ground plane of the fabricated prototypes is 127 mm $\times$ 203 mm. All designs except for the odd-mode reconfigurable patch were designed for high gain in the 2.45 GHz band, and use L between $55 - 59$ mm. Due to the diode placement necessary for the odd-mode reconfigurable design, use of shorted stubs would interfere with the ability to adjust DC bias voltage across the varactors. The shunt stubs were subsequently omitted resulting in a shorter length, $L = 38$ mm in order to resonate at a similar frequency.

5.1 Maximized Gain Patch Antenna

A resonant antenna at 2.45 GHz was designed using the proposed $k-\beta$ approach. Fig. 5.1 shows a photograph of the prototype antenna. The patch width was chosen to be $W = 30$ mm. The overall antenna length was chosen to be $L = 59$ mm, less than $\lambda_0/2 = 61.2$ mm by the fringe length. The stub parameters were set to $w_s = 1$ mm and $l_s = 3.9$ mm. The feed position is 5.5 mm from the middle of the patch, along the

center line through the width. The size of the ground plane is 305 mm $\times$ 305 mm. Simulation results were generated using Ansoft HFSS.

Simulation results for an infinite ground plane case are compared in order to exclude the effect of ground plane size on directivity. A patch with the described dimensions has a simulated directivity $D = 9.06$ dBi and a bandwidth BW $= 0.6\%$. A traditional patch of the same width and substrate, operating at the same frequency, has $D = 7.19$ dBi and BW $= 1.18\%$. The maximized gain patch, however, is longer as well as larger in width due to the extension of inductive stubs. A traditional patch on the same substrate having the same diagonal length has the dimensions $L = 39$ mm and $W = 58$ mm. This design has $D = 7.60$ dBi and BW $= 1.83\%$. These results show that, even when compared to a wider patch, the proposed design achieves an improvement of 1.46 dB in directivity.

A prototype of the maximum directivity design was built, measured, and then compared with simulated results which included finite ground plane size and conductor losses. Fig 5.2 shows an excellent agreement between the simulated and measured results for $|S_{11}|$. Far-zone realized gain patterns were measured and they are plotted in Fig. 5.3 together with simulated patterns. Good agreement is observed between simulated and measured patterns and broadside gains (measured: 7.12 dBi, simulated: 7.42 dBi). Cross-polarization level was measured to be better than 25 dB below co-pol at resonance. Using five cascaded unit-cells to build the patch, it was predicted that the structure would resonate at a unit-cell electrical length of 33.8°. The $k - \beta$ diagram predicts a resonance at 2.45 GHz. The resonant frequency of the measured patch is 2.455 GHz, giving a prediction error of only 0.2%. If the correction for the fringing length was neglected, the structure would have been predicted to resonate at $\beta l = 36°$. The associated resonance frequency is 2.543 GHz with an error of 3.58%. These results show that the unit cell design approach can provide an

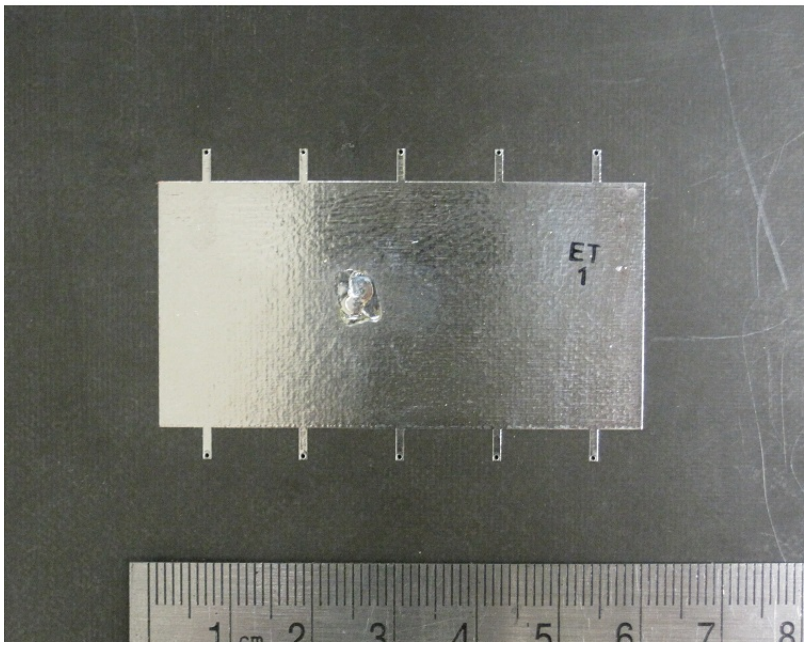

Figure 5.1: Photograph of the maximized gain patch prototype.

accurate resonant frequency prediction when the fringing length is taken into account in the design process.

5.2 Dual-Band Antenna

A dual-band antenna was designed for resonances at 2.405 GHz (odd-mode) and 2.849 GHz (even-mode), spaced by 84 MHz within the 2.4 GHz band. Four unit cells of length $l = 13.75$ mm were cascaded to realize the antenna. The specific values of the unit-cell parameters are given by $l_c = 9$ mm, $g = 0.254$ mm, and $l_s = 3$ mm. A photograph of the prototype is shown in Fig. 5.4. The overall antenna dimensions are 55 mm $\times$ 81 mm. A feed-probe is positioned 7 mm away from the patch center along the center line bisecting one patch in the x-direction.

The input impedance of the prototype was measured from 2.3 to 2.6 GHz in the lab using a vector network analyzer. The magnitudes of the input reflection coefficient $|S_{11}|$ are compared between simulated and measured results in Fig. 5.5, where an excellent agreement is observed in the entire measurement frequency range. Far-

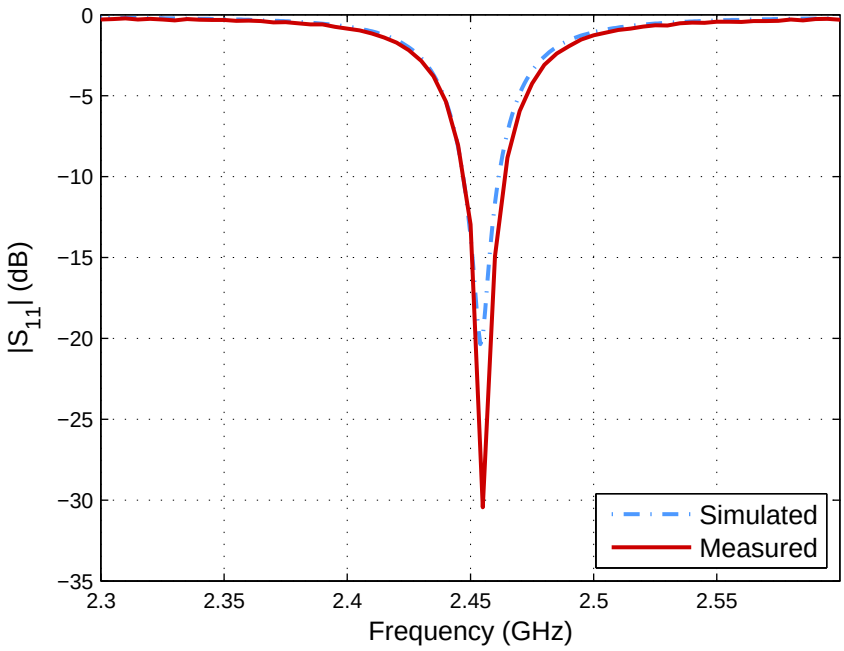

Figure 5.2: Simulated and measured responses for the input reflection coefficient of the maximized gain patch.

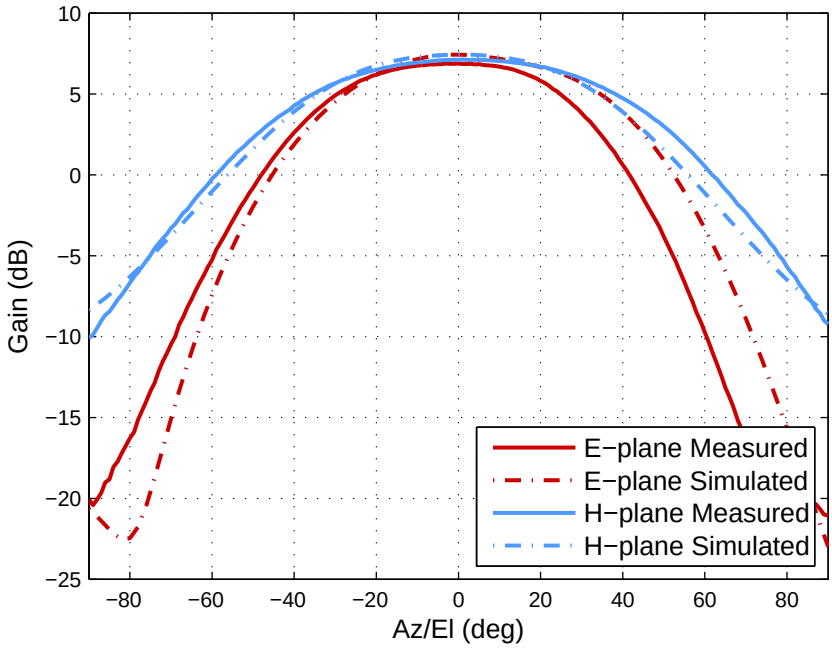

Figure 5.3: Simulated and measured realized gain patterns for the co-polarization component of the maximized gain patch in the principal planes.

zone radiation gain patterns were measured in an anechoic chamber. Fig. 5.6 plots the H-plane (the $y-z$ plane) realized gain patterns at the two resonance frequencies with respect to the angle θ measured from the $+z$-axis. Excellent agreement is observed at both frequencies except at angles close to $\theta = 90^\circ$ at the odd-mode frequency in Fig. 5.6(a). Characteristic differences in the even- and odd-mode patterns illustrated in Fig. 2.1(b) are clearly observed in Fig. 5.6. At the odd-mode frequency of 2.405 GHz, note that the magnitudes of the two major lobes are not equal and the pattern null is not located at θ=0° due to the presence of a residual even-mode component at this frequency. In contrast, the even-mode pattern in Fig. 5.6(b) is observed to be almost free of any odd-mode characteristic. This is due to a narrower bandwidth of the odd-mode resonance compared with the even-mode resonance. E-plane cuts for realized gain are plotted in Fig. 5.7. Measured beamwidth at the even-mode resonance is a few degrees wider than simulated. Due to the small ground plane size in the E-plane, the patch is sensitive to tolerances in this dimension. This effect was minimized in the maximized gain patch measurements by backing the patch with a larger ground plane. Because this beamwidth is not critical for the coupled designs, they were measured without an extended ground plane. As the odd-mode pattern has a null in the entire E-plane, measurements at this resonance are very sensitive to the depth and precise location of the null. Measured gain value is seen to be higher than the simulated value in Fig. 5.7(a) due to this sensitivity. The cross-polarization levels are typically better than 20 dB below the co-polarized levels. The worst case is at the odd-mode resonance in the E-plane where the cross-polarized level comes as high as 16 dB below the peak co-polarized value.

5.3 Wide-Band Antenna

The antenna design method allows the two resonance frequencies to be separated by an arbitrarily small difference due to the uncoupled nature of the even and odd

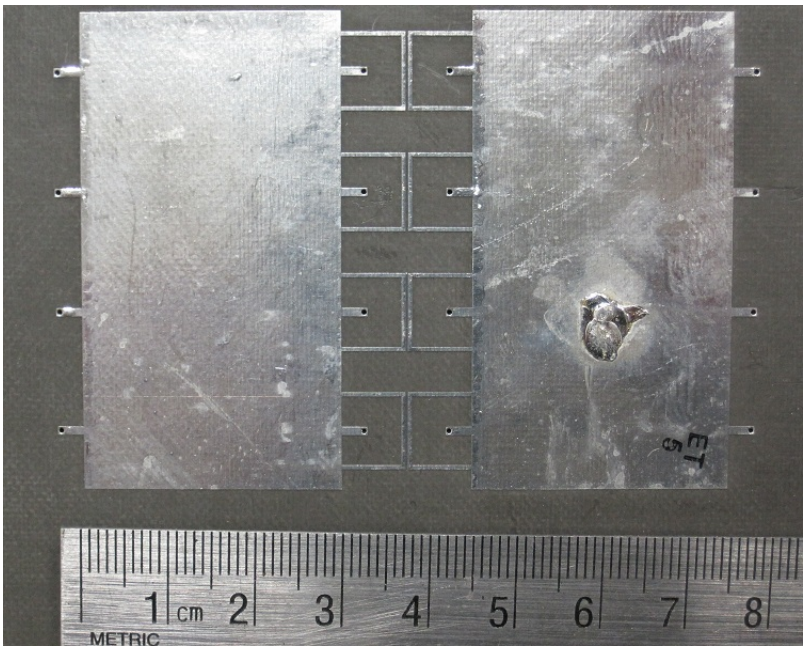

Figure 5.4: Photograph of the dual-band antenna prototype.

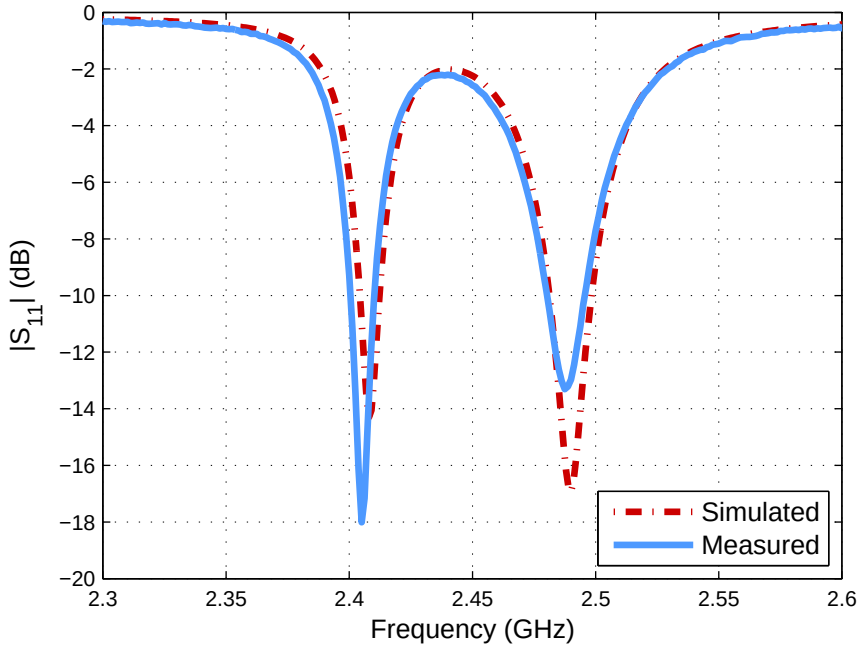

Figure 5.5: Simulated and measured responses for the input reflection coefficient of the dual-band patch.

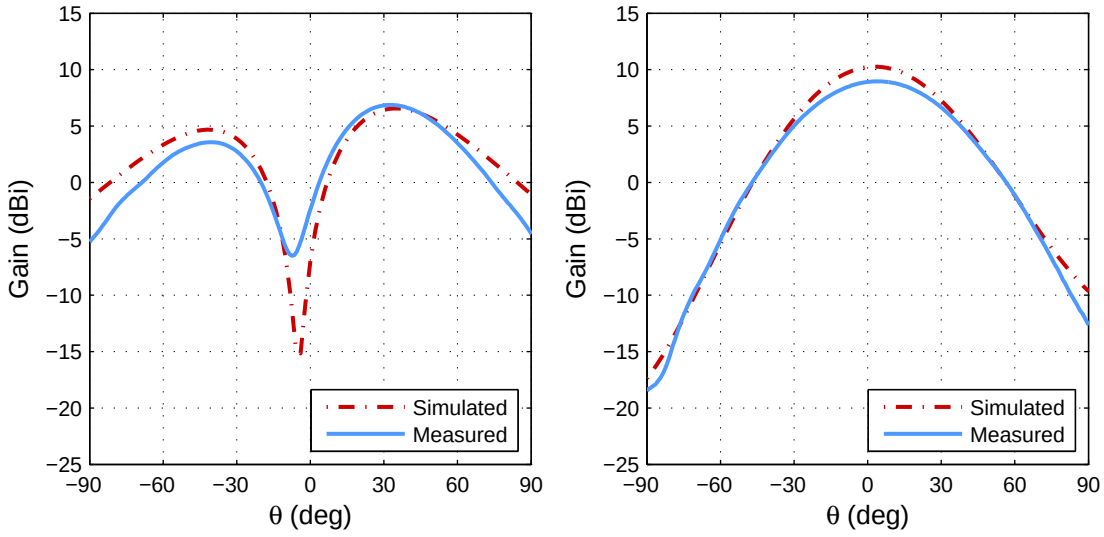

(a) (b)

Figure 5.6: The H-plane realized gain patterns for the co-polarization component of the dual-band design. (a) Odd-mode resonance (2.405 GHz). (b) Even-mode resonance (2.489 GHz).

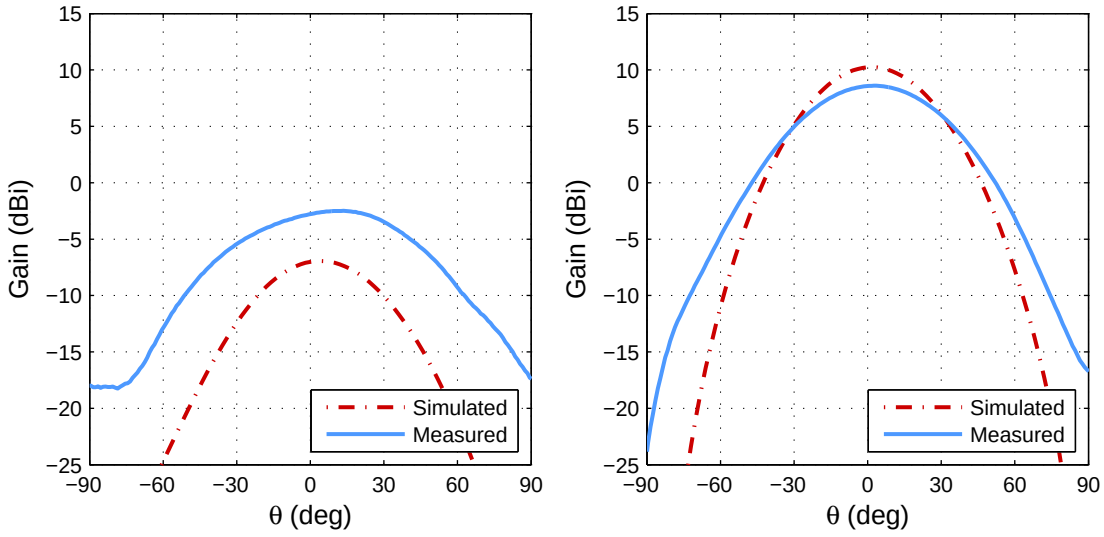

(a) (b)

Figure 5.7: The E-plane realized gain patterns for the co-polarization component of the dual-band design. (a) Odd-mode resonance (2.405 GHz). (b) Even-mode resonance (2.489 GHz).

modes of coupled transmission lines. By bringing the two resonance frequencies closer to each other, an antenna can be designed to have a wider impedance bandwidth than a similar single resonance patch. A wide-band antenna was designed around the center frequency of 2.45 GHz by cascading five unit cells with $l = 11$ mm. The unit-cell geometrical parameters were chosen to be $l_c = 5$ mm, $g = 0.3$ mm, and $l_s = 4.5$ mm. The overall dimensions of the antenna are 55 mm $\times$ 84 mm. A single probe feed is located at 6.5 mm away from the center of the excited patch. A photograph of the prototype is shown in Fig. 5.8. From Fig. 2.3(a) and 2.3(b), weaker coupling between the two patches leads to a narrower separation between the two resonance frequencies. For this wide-band design, note that g is larger and l_c is shorter than their respective counterpart in the dual-band design. Additionally, a smaller loop allows a shorter unit-cell size, leading to a five-cell structure rather than the four-cell geometry of the previous design.

Fig. 5.9 compares the simulated and measured reflection coefficient for the wide-band antenna. Excellent agreement is obtained over the entire frequency range. Two resonances are clearly visible, and $|S_{11}|$ stays below -10 dB over the merged band. The 2 : 1 VSWR bandwidth of the merged resonances is found to be 36 MHz , or 1.46%. The H-plane gain patterns for the co-polarized component are plotted at three different frequencies in Fig. 5.10. Good agreement is obtained between simulation and measurement at each frequency. For this design, the radiation pattern is a strong function of frequency within the band. Frequency points in the low, mid, and high range in the band were chosen in Fig. 5.10. At the low frequency of 2.436 GHz, Fig. 5.10(a) shows a pattern characteristic of the odd mode. At the mid-band frequency of 2.457 GHz, a highly asymmetric pattern is obtained. At the high-band frequency of 2.471 GHz, the even-mode radiation characteristics dominate as shown in Fig. 5.10(c). E-plane cuts for realized gain plotted in Fig. 5.11 show similar results to those seen in the case of the dual-band antenna. The cross-polarization levels were

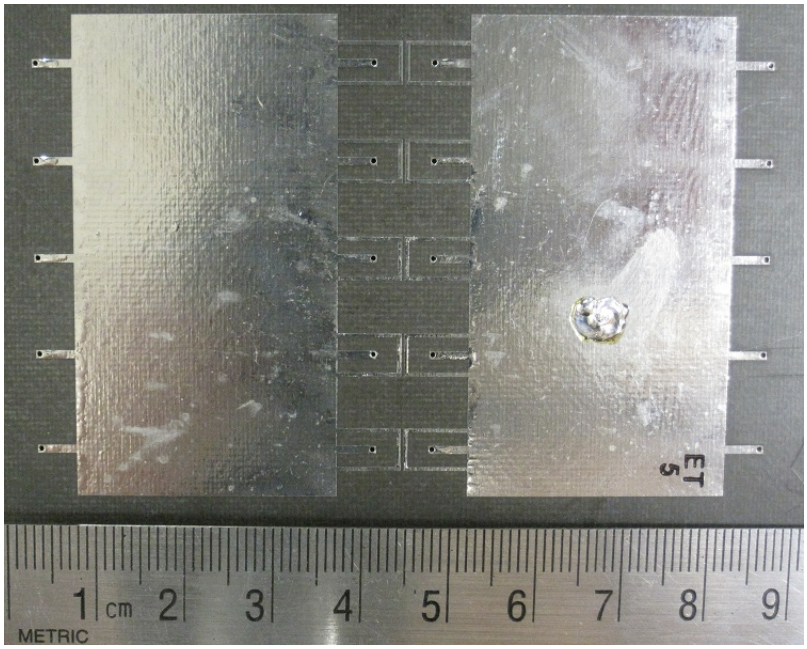

Figure 5.8: Photograph of the wide-band antenna prototype.

measured to be between $25 - 30$ dB below the co-polarization levels throughout the impedance bandwidth of this antenna.

5.4 Pattern Reconfigurable Antenna

A pattern reconfigurable antenna was designed by placing a Skyworks Solutions, Inc. SMV1234-079LF varactor diode in series with each shunt inductive stub to ground. In this configuration, the diode capacitance loads both modes. As DC bias voltage is increased, the resonances shift upward in frequency. This antenna was designed with the two resonances spaced such that either could be selected to occur at 2.45 GHz. The bias voltage was applied through the coax feed and transferred to the parasitic patch by an RF choke inductor.

The dimensions of this design are $W = 30$ mm, $L = 55$ mm, $s = 15$ mm, $l_c = 6$ mm, and $g = 0.3$ mm . Stubs have overall length $l_s = 4.7$ mm, with varactor diodes placed 0.9 mm from the patch edge across a $0.9 -$ mm gap. Five unit cells were

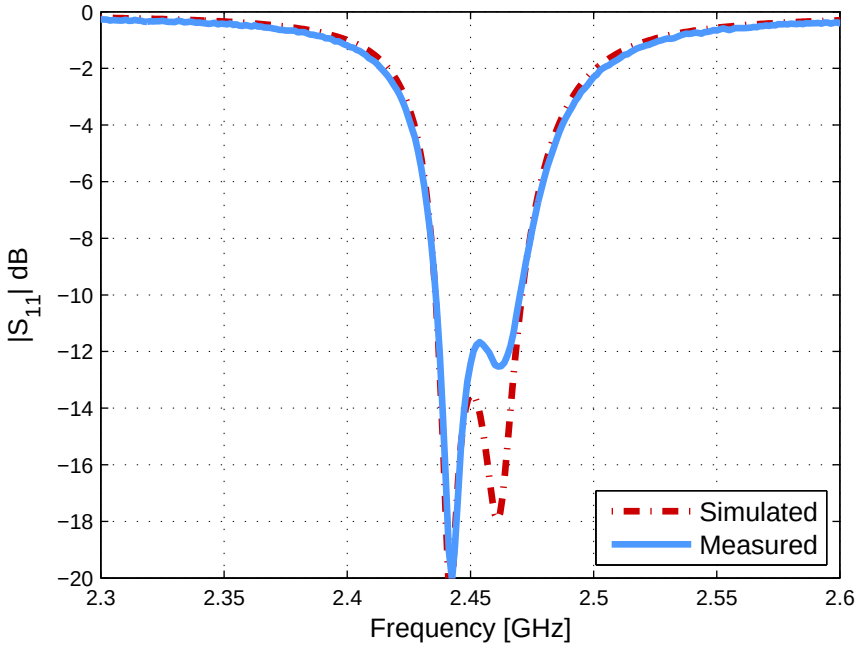

Figure 5.9: Simulated and measured responses for the input reflection coefficient of the wide-band patch.

cascaded to form the antenna, and a varactor diode was placed on each stub of every unit cell. The probe feed was located 6.5 mm from the center of the driven patch.

In simulation, a series LC circuit was used to represent the variable capacitance and parasitic package inductance of the diode. Ability to select either resonance at 2.45 GHz by adjusting bias voltage was confirmed in measurement. However, comparisons with simulation results for S_{11} in Fig. 5.13 and radiation pattern in Fig. 5.14 show poor agreement. Neglecting the parasitic resistance in the diode model was found to be the primary source of inaccuracy. Simulation results using a series RLC varactor model are also plotted in Figs. 5.13, 5.14, and 5.15, which show much better agreement with measured responses. The resistance of the diodes has a significant effect on efficiency, reducing G_R. This causes the odd-mode pattern to be skewed by the even-mode radiation and poorly defined. This antenna could be redesigned by taking loss into account and spacing the resonances slightly further apart to improve the odd-mode pattern. Far-field radiation patterns in Figs. 5.14

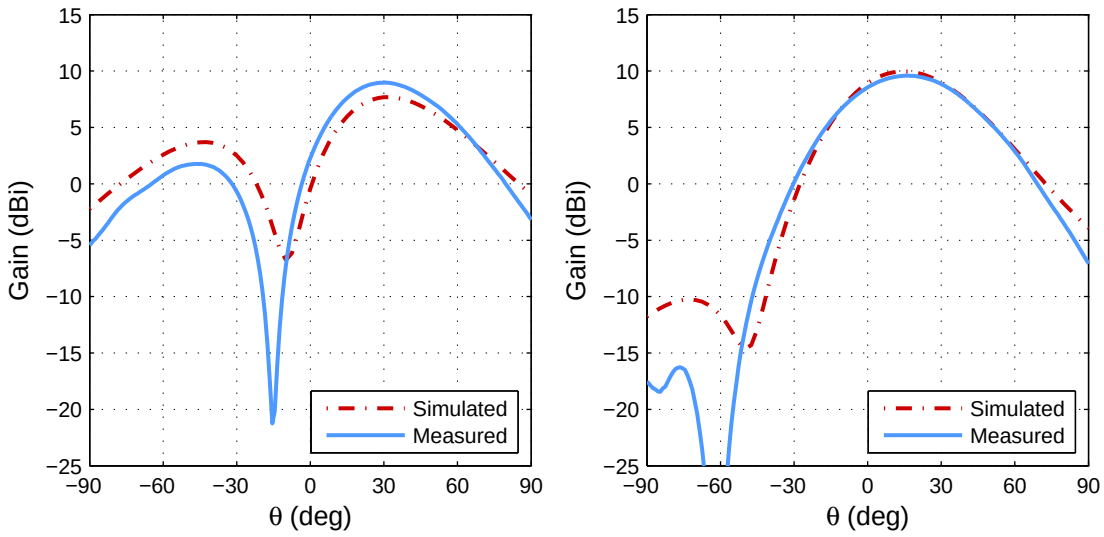

(a)

(b)

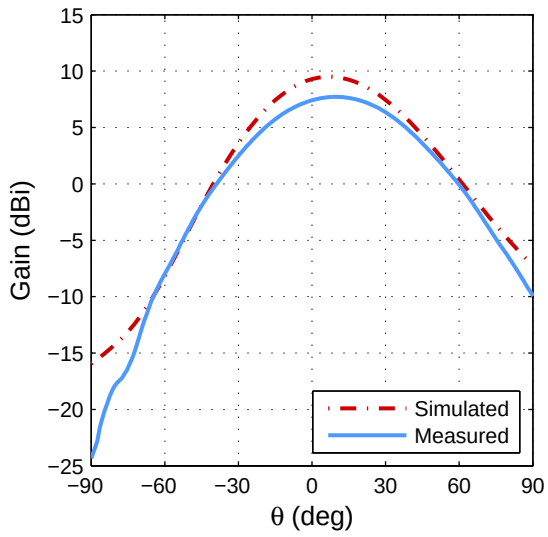

(c)

Figure 5.10: The H-plane realized gain patterns for the co-polarization component of the wide-band design. (a) At 2.436 GHz. (b) At 2.457 GHz. (c) At 2.471 GHz.

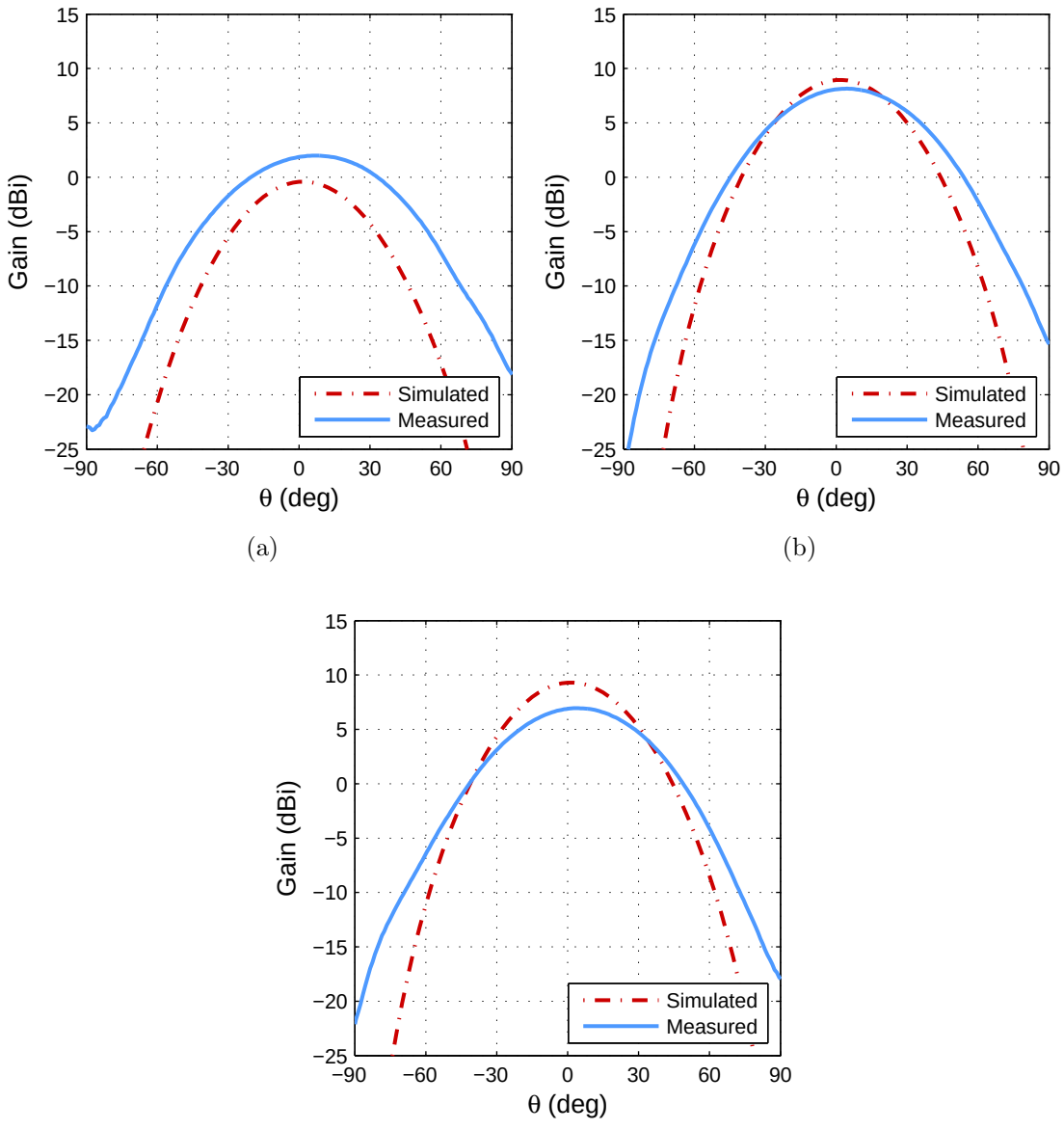

(a) (b)

(c)

Figure 5.11: The E-plane realized gain patterns for the co-polarization component of the wide-band design. (a) At 2.436 GHz. (b) At 2.457 GHz. (c) At 2.471 GHz.

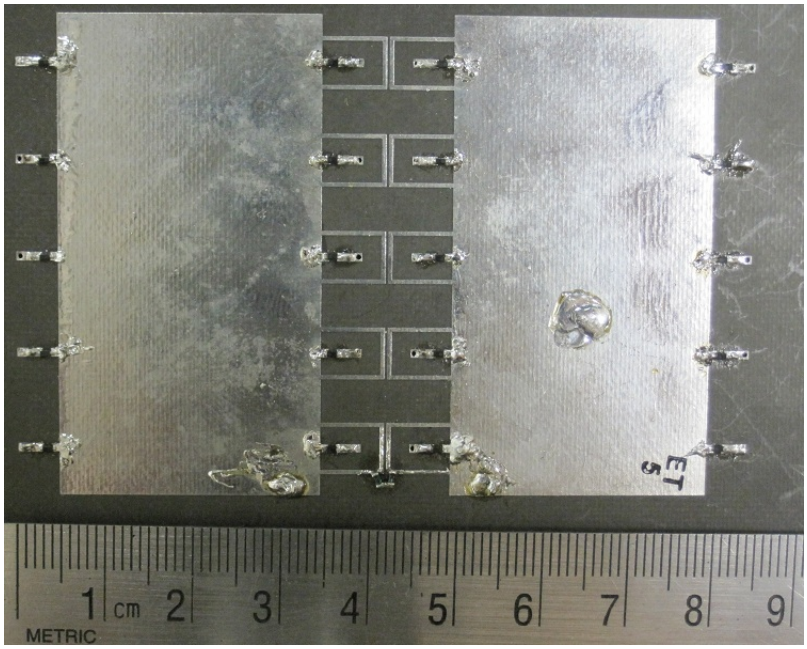

Figure 5.12: Photograph of the pattern-reconfigurable antenna prototype.

and 5.15 show good agreement between simulation and measurement results when loss is included, particularly in the H-plane. Cross-polarization level at 2.45 GHz was measured to be 20 dB below co-pol with the odd-mode pattern selected and 24.5 dB below co-pol with the even-mode pattern selected.

5.5 Odd-Mode Reconfigurable Antenna

This design uses four unit cells and has dimensions of $W = 26$ mm, $L = 38$ mm, $s = 15$ mm, $l_c = 8.5$ mm, and $g = 0.254$ mm (10 mil). The overall dimensions of the antenna are 38 mm $\times$ 75 mm. The trace width of the coupling loops along the symmetry plane is increased from 0.5mm to 0.823 mm with notches placed in the center to accommodate the 0.9 mm length of the SMV1234-079LF varactor diodes. Inductive stubs are not used on this design as they would interfere with ability to bias the diodes in this configuration. Because stubs are not used to improve gain, patch length is shorter than the other designs.

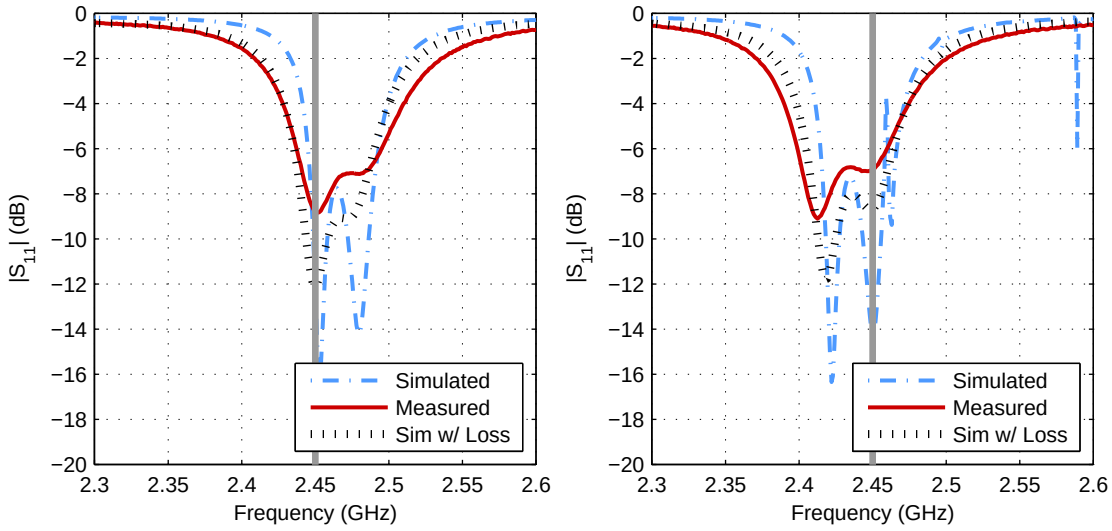

(a) (b)

Figure 5.13: Predicted and measured input reflection coefficient response for the pattern-reconfigurable design. The design frequency is indicated by a solid vertical line in gray in each plot. (a) Odd-mode resonance at 2.45 GHz. (b) Even-mode resonance at 2.45 GHz.

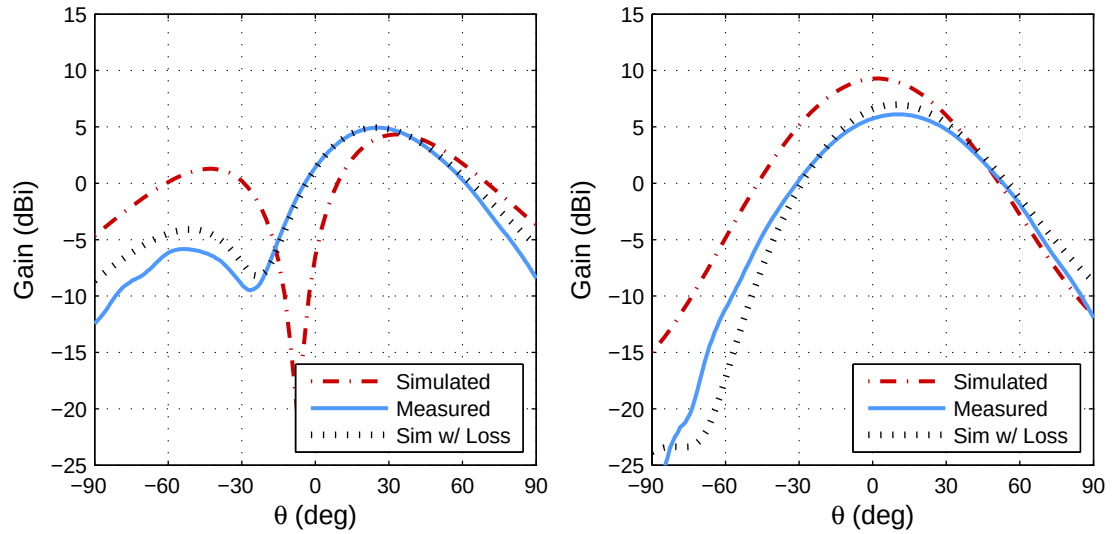

(a) (b)

Figure 5.14: Pattern-reconfigurable design co-pol absolute gain in H-plane. (a) Odd-mode resonance at 2.45 GHz. (b) Even-mode resonance at 2.45 GHz.

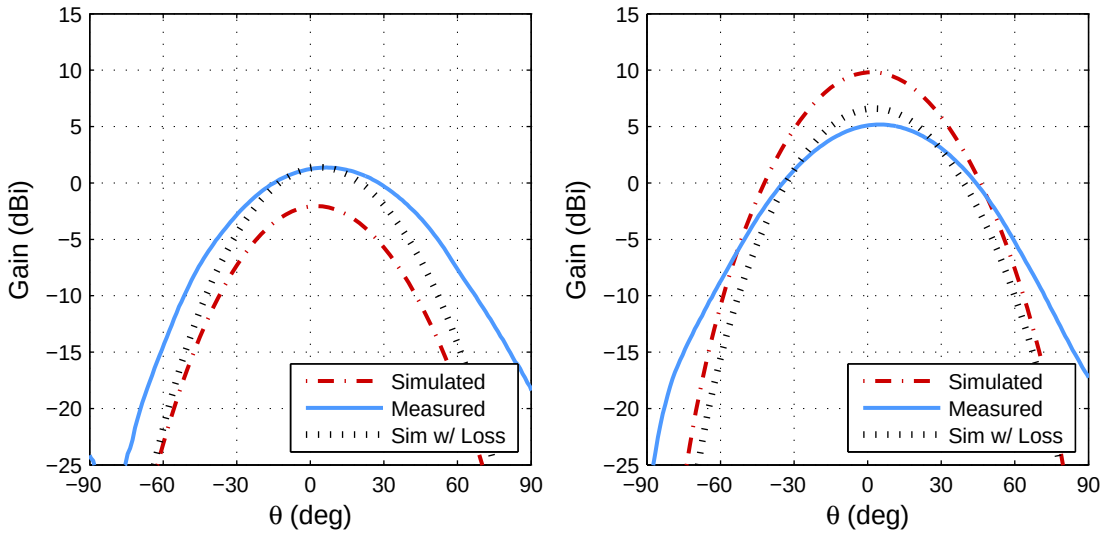

Figure 5.15: Pattern-reconfigurable design co-pol absolute gain in E-plane. (a) Odd-mode resonance at 2.45 GHz. (b) Even-mode resonance at 2.45 GHz.

The design goal was to maintain constant frequency and radiation pattern of the even-mode resonance while shifting the odd-mode frequency by varying DC bias voltage. Reflection coefficient plotted in Fig. 5.17(a) shows a simulated frequency tuning range of 3.84%, although measurement results of Fig. 5.17(b) were only able to achieve a 1.86% shift from 2.8 to 2.85 GHz. The diode is being operated slightly above its specified frequency range, possibly limiting its capacitive range. Fig. 5.18 shows that the radiation pattern of the even-mode is unaffected by tuning of the odd-mode. Simulated gain data was not shown in Figs. 5.18 and 5.19 to avoid cluttering the plots, but showed similar agreement as seen in the dual-band and wide-impedance designs. Cross-polarization levels were measured to be 25 dB below co-pol values at the even-mode resonance, and at least 15 dB below co-pol at odd-mode resonance throughout the tunable range.

The parasitic resistance of the varactor was taken into account when designing this antenna. With this improved diode model, a good agreement is seen between

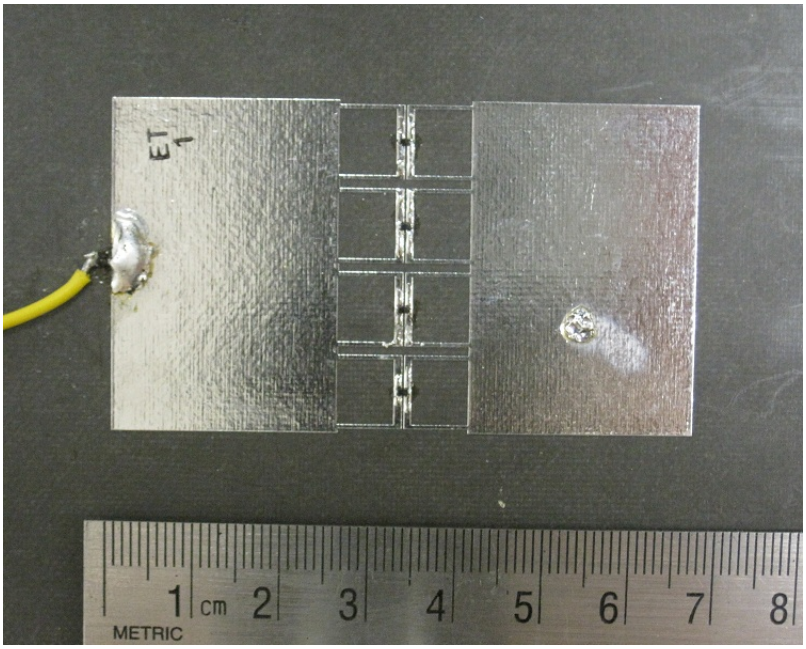

Figure 5.16: Photograph of the odd-mode-reconfigurable antenna prototype.

simulation and measurement results. The even-mode resonance occurred about 1% above prediction, but was extremely stable in frequency and pattern over the range of DC bias values tested. The odd-mode resonance occurred in the predicted band, but with a narrower tunable range. Also, because fewer varactor diodes were used in this design than the patter-reconfigurable antenna (4 instead of 20), the gain is higher for the odd-mode reconfigurable prototype.

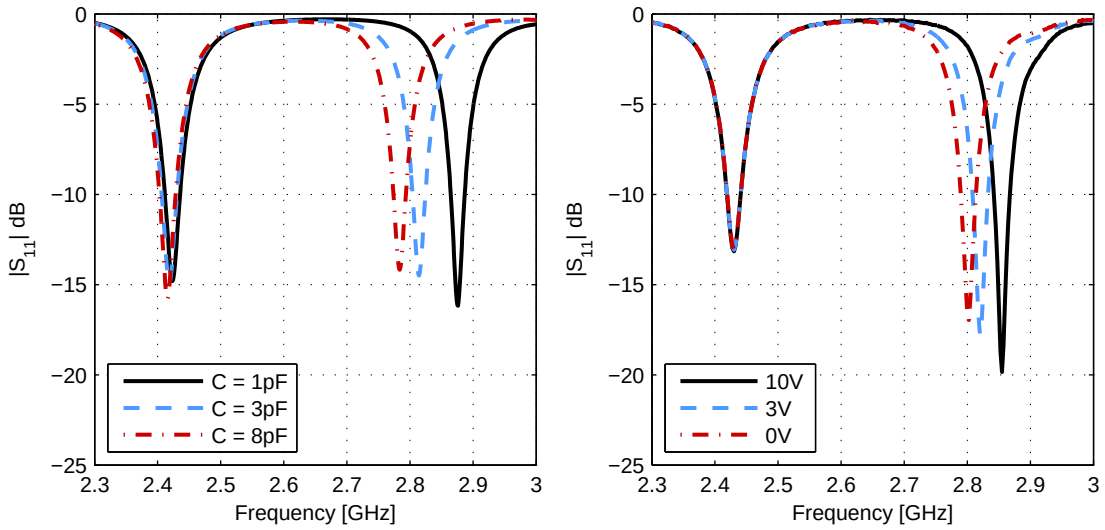

(a) (b)

Figure 5.17: Simulated (a) and measured (b) responses for the input reflection coefficient of the frequency reconfigurable design.

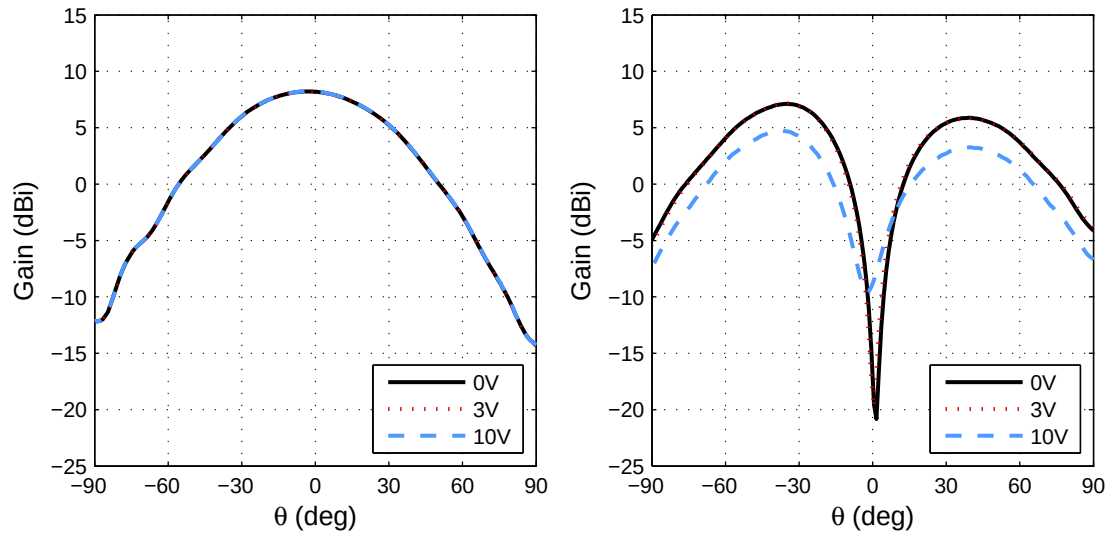

(a) (b)

Figure 5.18: Measured H-plane realized gain patterns for the co-polarization component of the frequency reconfigurable design at even-mode (a) and odd-mode resonance (b).

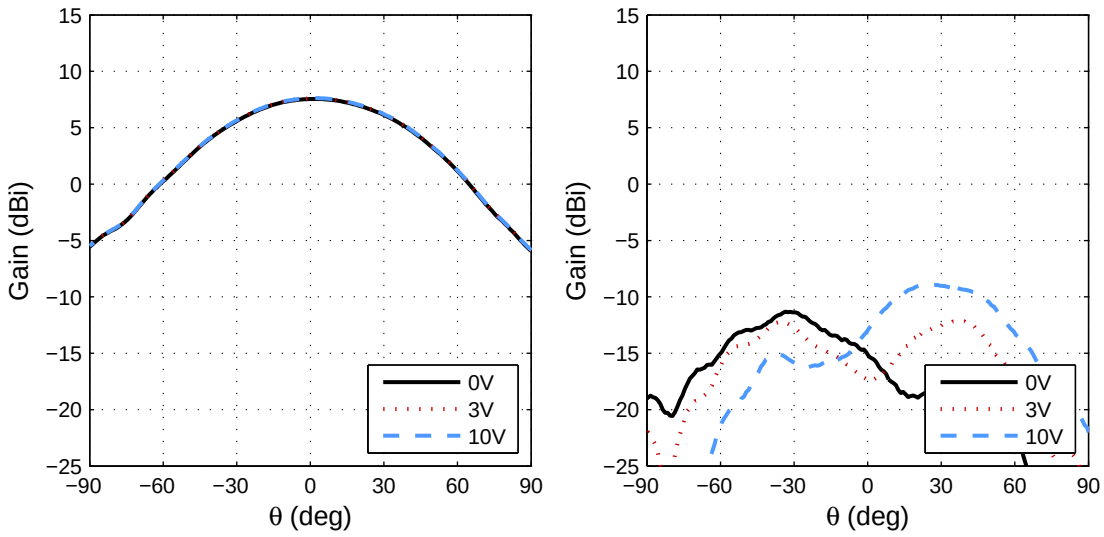

Figure 5.19: Measured E-plane realized gain patterns for the co-polarization component of the frequency reconfigurable design at even-mode (a) and odd-mode resonance (b).

CHAPTER 6

FUTURE WORK

The work presented in this thesis represents an exploration of a new antenna topology. The goals were to design and realize coupled-TL based patch antennas and verify their operation through measurement results. This chapter will comment on portions of the work presented that could be expanded for future research.

One area that could be investigated is limits on the patch width in the maximum directivity patch. The design chosen used shorted shunt stubs in order to realize shunt inductance, as this gave very predictable results. The patch width was also chosen to be 30 mm for consistency across the fabricated designs. Using a wider patch width would necessitate shorter stubs. In the limit, inductance would be realized with a via to ground right on the edge of the patch. No longer having a stub as the tuning variable, β could be tuned by adjusting W and substrate thickness. Using this technique H-plane beamwidth could be narrowed, further enhancing the directivity.

Another area that has not been explored is adding a tunable feed network to a coupled patch design. This network would split the input and feed both elements. Tuning the phase between the two element excitations would allow a control over the relative difference between even- and odd-mode radiation resistances. The results of Chapter 5 show that the radiation patterns show an asymmetry due to both modes being excited simultaneously. By controlling this ratio of excitation some range of adaptive nulling could be realized. The proposed method would retain the single input port, and the included network could be a varactor loaded hybrid. In this way a DC offset on the feed could tune the null angle. If a method was devised

to control this technique in conjunction with the pattern-reconfigurable design, even better control over radiation pattern would be possible.

As a final thought, reactively loading the second port at the symmetric location from the single excitation port with respect to the symmetry plane has not been explored. The only cases considered have been a perfect open which makes the input impedance Z_{in} equal to the average of even- and odd-mode impedances. It is possible that an improvement in bandwidth, a better control of the total pattern, or further tunability options could be obtained with this configuration.

CHAPTER 7

CONCLUSION

Novel resonant printed antenna designs based on coupled TL-metamaterial structure have been presented. The design exploits the nature of coupled TLs of symmetric construction to configure the even- and odd-mode resonance frequencies independently of each other. In particular, a coupling structure based on thin loops allows the two transmission lines to be separated so that the odd-mode current can radiate efficiently. A series of shunt inductive stubs can modify the phase constants such that the overall length of the antenna can be adjusted closer to a half free-space wavelength, leading to a high gain. Four coupled-line antennas – a dual-band antenna, a wide-band antenna, an odd-mode reconfigurable antenna, and a pattern-reconfigurable antenna – as well as one single patch with a maximized gain were designed, fabricated, and experimentally characterized. Excellent agreement was obtained between simulated and measured results for the dual-band, wide-band, and maximized-gain antenna designs, validating the proposed design approach. Inaccuracies in the varactor diode circuit model at the design frequency of 2.45 GHz resulted in some discrepancy between predicted and measured responses for the pattern- and frequency-reconfigurable antennas; however, the abilities to tune the pattern and the resonance frequency were clearly demonstrated. The proposed antenna design approach may find applications where a choice is desired in the radiation pattern among the anti-symmetric odd-mode pattern with a broadside pattern null, the symmetric even-mode pattern with a broadside pattern maximum, and an asymmetric pattern resulting from a superposition of the two patterns. The selection of a pattern

in the wide-ranging characteristics may be made in real time using a single control voltage.

A technique for maximizing the gain of a rectangular patch antenna has been applied to this coupled-line topology. Using a metamaterial-inspired design approach, the conditions for the maximum directivity are met. Simulation and measurement results confirm the expected increase in directivity, and corresponding gain. Additionally, this technique has a greater effect on gain improvement when the effects of a finite ground plane are taken into account. This is an important attribute when the ground plane size is limited. Although this phase engineering can increase the gain of microstrip patch antennas to be comparable to that of a patch on an air substrate, it is noted that it achieves a gain enhancement at the expense of a decrease in bandwidth. This effect has been demonstrated in the maximum-gain patch antenna.

BIBLIOGRAPHY

[1] D. M. Pozar and D. H. Schaubert, *Microstrip Antennas*. Piscataway, NJ: IEEE Press, 1995.

[2] D. M. Pozar, *Microstrip Antennas*. Piscataway, NJ: IEEE Press, 1995, ch. 3 A Review of Bandwidth Enhancement Techniques for Microstrip Antennas, pp. 157–165.

[3] R. Q. Lee and K.-F. Lee, "Experimental study of the two-layer electromagnetically coupled rectangular patch antenna," *IEEE Trans. Antennas Propag.*, vol. 38, pp. 1298–1302, Aug. 1990.

[4] C.-L. Mak, H. Wong, and K.-M. Luk, "High-gain and wide-band single-layer patch antenna for wireless communications," *IEEE Trans. Veh. Technol.*, vol. 54, pp. 33–40, Jan. 2005.

[5] D. Loffler, Y. Venot, and W. Wiesbeck, "Low cost broadband antenna with sdma capability for next generation pcs base stations," in *Proc. 29th Eur. Microw. Conf.*, Rome, Italy, 1999, pp. 142 –145.

[6] Y. Qian, R. Coccioli, D. Sievenpiper, V. Radisic, E. Yablonovitch, and T. Itoh, "A microstrip patch antenna using novel photonic band-gap structures," *Microw. J.*, vol. 42, pp. 66–71, Jan. 1999.

[7] S. Chattopadhyay, J. Y. Siddiqui, and D. Guha, "Rectangular microstrip patch on a composite dielectric substrate for high-gain wide-beam radiation patterns," *IEEE Trans. Antennas Propag.*, vol. 57, pp. 3324–3327, Oct. 2009.

[8] D. H. Schaubert, F. G. Farrar, S. T. Hayes, and A. R. Sindoris, "Frequency-agile, polarization diverse microstrip antennas and frequency scanned arrays," US Patent 4,367,474, to the United States of America as represented by the Secretary of the Army, 1983.

[9] N. Behdad and K. Sarabandi, "Dual-band reconfigurable antenna with a very wide tunability range," *IEEE Trans. Antennas Propag.*, vol. 54, no. 2, pp. 409 – 416, Feb. 2006.

[10] J.-W. Baik, S. Pyo, T.-H. Lee, and Y.-S. Kim, "Switchable printed Yagi-Uda antenna with pattern reconfiguration," *ETRI J.*, vol. 31, pp. 318–320, Jun. 2009.

[11] S. Zhang, G. H. Huff, J. Feng, and J. T. Bernhard, "A pattern reconfigurable microstrip parasitic array," *IEEE Trans. Antennas Propag.*, vol. 52, no. 10, pp. 2773 – 2776, 2004.

[12] D. Rodrigo, Y. Damgaci, N. Biyikli, B. A. Cetiner, J. Romeu, and L. Jofre, "Mems-reconfigurable antenna based on a multi-size pixelled geometry," in *Proc. 2010 Eur. Conf. Antennas Propag. (EuCAP)*, 2010, pp. 1 –4.

[13] C. Jung, M. Lee, G. P. Li, and F. D. Flaviis, "Reconfigurable scan-beam single-arm spiral antenna integrated with rf-mems switches," *IEEE Trans. Antennas Propag.*, vol. 54, no. 2, pp. 455 – 463, Feb. 2006.

[14] B. A. Cetiner, H. Jafarkhani, J.-Y. Qian, H. J. Yoo, A. Grau, and F. D. Flaviis, "Multifunctional reconfigurable mems integrated antennas for adaptive mimo systems," *IEEE Commun. Mag.*, vol. 42, no. 12, pp. 62 – 70, 2004.

[15] G. H. Huff and J. T. Bernhard, "Integration of packaged rf mems switches with radiation pattern reconfigurable square spiral microstrip antennas," *IEEE Trans. Antennas Propag.*, vol. 54, no. 2, pp. 464 – 469, Feb. 2006.

[16] A. C. K. Mak, C. R. Rowell, R. D. Murch, and C.-L. Mak, "Reconfigurable multiband antenna designs for wireless communication devices," *IEEE Trans. Antennas Propag.*, vol. 55, no. 7, pp. 1919 –1928, Jul. 2007.

[17] Skyworks Solutions, Inc., "Varactor diodes," Aug 2008, 200824 Rev. A.

[18] C. Caloz and T. Itoh, *Electromagnetic Metamaterials*. New York: Wiley, 2005.

[19] D. M. Pozar, *Microwave Engineering*, 3rd ed. Hoboken, NJ: Wiley, 2005.

[20] K. C. Gupta, R. Garg, I. Bahl, and P. Bhartia, *Microstrip Lines and Slotlines*. Boston: Artech House, 1996.

[21] C. A. Balanis, *Antenna Theory Analysis and Design*. Hoboken, NJ: Wiley, 2005.